T. R.
VAN YUZUNCU YIL UNIVERSITY
INSTITUTE OF NATURAL AND APPLIED SCIENCES
DEPARTMENT OF PHYSICS

THE INVESTIGATION OF SOME PHYSICAL PROPERTIES OF $BaIrO_3$ PEROVSKITE CRYSTAL WITH DENSITY FUNCTIONAL THEORY

M.Sc. THESIS

PREPARED BY: Hawzhi Rzgar SOR
SUPERVISOR : Assoc. Prof. Dr. Emel KILIT DOĞAN

VAN-2021

T. R.

VAN YUZUNCU YIL UNIVERSITY
INSTITUTE OF NATURAL AND APPLIED SCIENCES
DEPARTMENT OF PHYSICS

THE INVESTIGATION OF SOME PHYSICAL PROPERTIES OF $BaIrO_3$ PEROVSKITE CRYSTAL WITH DENSITY FUNCTIONAL THEORY

M.Sc. THESIS

PREPARED BY: Hawzhin Rzgar SOR

VAN-2021

ACCEPTANCE and APPROVAL PAGE

This thesis entitled "**THE INVESTIGATION OF SOME PHYSICAL PROPERTIES OF BaIrO3 PEROVSKITE CRYSTAL WITH DENSITY FUNCTIONAL THEORY**" presented by Hawzhin Rzgar SOR under supervision of Assos. Prof. Dr. Emel KİLİT DOĞAN in the department of Physics has been accepted as a M. Sc. thesis according to Legislations of Graduate Higher Education on 24/08/2021 with majority of votes members of jury.

Chair: Assoc. Prof. Dr. Hakan GÜNDOĞMUŞ Signature:

Member: Assoc. Prof. Dr. Sinem ERDEN GÜLEBAĞLAN Signature:

Member: Assoc. Prof. Dr. Emel KİLİT DOĞAN Signature:

This thesis has been approved by the committee of The Institute of Natural and Applied Science on 21/09/2021 with decision number 2021/45-I

Signature

……………..………..

Director of Institute

THESIS STATEMENT

All information presented in the thesis obtained in the frame of ethical behavior and academic rules. In addition all kinds of information that does not belong to me have been cited appropriately in the thesis prepared by the thesis writing rules.

Hawzhin SOR

ABSTRACT

THE INVESTIGATION OF SOME PHYSICAL PROPERTIES OF $BaIrO_3$ PEROVSKITE CRYSTAL WITH DENSITY FUNCTIONAL THEORY

SOR, Hawzhin Rzgar
M. Sc. Thesis, Department of Physics
Supervisor: Assoc. Prof. Dr. Emel KILIT DOĞAN
September 2021, 69 pages

In this thesis the structural, electronic and elastic properties of $BaIrO_3$ perovskite crystal is studied theoretically by Density Functional Theory within both Generalized Gradient Approximation and Local Density Approximation. The computation is performed mainly by using the ABINIT computer programme. However, for sketching the unit cell structure, calculating the bonds and the bond lengths the Vesta computer programme is used.

In order to perform those calculations first the cut-off energy and the k-point optimisations are done. Afterwards, we investigated the structural properties of $BaIrO_3$ cubic crystal. The lattice parameter is calculated theoretically and it is noticed that it is very close to the value that is obtained from the literature. The unit cell, bonds and the bond lenghts of this crystal is also computed. The total energy, volume and the volume vs. pressure behaviour exhibited for the ground state in this study. After the electronic property calculations, the electronic band structure, density of states and partial density of states graphs are plotted. It ıs seen that $BaIrO_3$ is a good conductor. The computation of elastic properties revealed that $BaIrO_3$ is mechanically stable material. $BaIrO_3$ crystal is an elastic and elastically isotropic in structure.

Since all those calculations are done for the first time, we believe that this study will shed light on the new studies on $BaIrO_3$ cubic crystal.

Keywords: ABINIT, $BaIrO_3$, Density functional theory, Density of states, Elastic properties, Electronic properties, Partial density of states.

ÖZET

PEROVSKİT $BaIrO_3$ KRİSTALİNİN BAZI FİZİKSEL ÖZELLİKLERİNİN YOĞUNLUK FONKSİYONELİ TEORİSİ İLE İNCELENMESİ

SOR, Hawzhin Rzgar
Yüksek Lisans Tezi, Fizik Anabilim Dalı
Tez Danışmanı: Doç. Dr. Emel KİLİT DOĞAN
Eylül 2021, 69 sayfa

Bu tezde, $BaIrO_3$ perovskite kristalinin yapısal, elektronik ve elastik özellikleri, hem Genelleştirilmiş Gradyent Yaklaşımı hem de Yerel Yoğunluk Yaklaşımı kapsamında Yoğunluk Fonksiyonel Teorisi ile teorik olarak incelenmiştir. Hesaplama esas olarak ABINIT bilgisayar programı kullanılarak yapmıştır. Ancak birim hücre yapısının çizilmesi, bağların ve bağ uzunluklarının hesaplanması için Vesta bilgisayar programı kullanılmıştır.

Bu hesaplamaları yapabilmek için öncelikle kesme enerjisi ve k noktası optimizasyonları yapılmıştır. Daha sonra $BaIrO_3$ kübik kristalin yapısal özellikleri araştırılmıştır. Örgü parametresi teorik olarak hesaplanmış ve literatürden elde edilen değere çok yakın olduğu görülmüştür. Bu kristalin birim hücresi, bağları ve bağ uzunlukları da hesaplanmıştır. Bu çalışmada temel durum için toplam enerji, hacim ve hacim-basınç davranışı da hesaplanmıştır. Elektronik özellik hesaplamalarından sonra elektronik bant yapısı, durum yoğunluğu ve durumların kısmi yoğunluğu grafikleri çizilmiştir. $BaIrO_3$'ün iyi bir iletken olduğu görülmüştür. Elastik özelliklerin hesaplanması, $BaIrO_3$'ün mekanik olarak kararlı bir malzeme olduğunu ortaya çıkardı. Ayrıca $BaIrO_3$ kristali elastik ve elastik olarak izotropik yapıdadır.

Tüm bu hesaplamalar ilk defa yapıldığı için bu çalışmanın $BaIrO_3$ kübik kristal ile ilgili yeni çalışmalara ışık tutacağını düşünüyoruz.

Anahtar kelimeler: ABINIT, $BaIrO_3$, Durum yoğunluğu, Elastik özellikler, Elektronik özellikler, Kısmı durum yoğunluğu, Yoğunluk fonksiyoneli teorisi.

ACKNOWLEDGMENT

First and foremost, I would like to praise Allah the Almighty, the Most Gracious, and the Most Merciful for His blessing given to me during my study and in completing this thesis. May Allah’s blessing goes to His final Prophet Muhammad (peace be up on him), his family and his companions.

I would like to express my gratitude to my primary supervisor, Dr. Emel, who guided me throughout this project realy i love her with deep of my heart, whithout her helping it is imposible to get MSc degree she is a big knewlodge donor. Also, i wish to extend my thanks to my sweet husband for his all efforts during my study. I wish to show my appreciation to my only brother in life Hawraman gian for his financially support. My deepest gratitude goes to all of my childern my dear son Wanyar and my little girl Nwa.

2021

Hawzhin Rzgar Sor

TABLE OF CONTENTS

Page

ABSTRACT ... i
ÖZET ... iii
ACKNOWLEDGMENT ... v
TABLE OF CONTENTS ... vii
LIST OF TABLES ... iix
LIST OF FIGURES ... xi
SYMBOLS AND ABBREVIATIONS ... xiiiiii
1. INTRODUCTION ... 1
2. LITERATURE REVIEW ... 3
3. THEORETICAL BACKGROUND ... 5
3.1. Classification of Solids and Crystal Structure ... 5
3.1.1. Crystal structure ... 6
1.1.3. Types of crystal lattice ... 7
1.1.4. One dimensional crystal ... 7
1.1.5. Two dimensional crystal ... 8
1.1.5. Three dimensional crystal ... 8
3.2. Diffraction in Crystals and Bragg's Law ... 9
3.3. Reciprocal Lattice ... 10
3.4. Brillouin Zone ... 11
3.5. Electronic Band Structure in Crystals ... 12
3.6. Density of States (DOS) ... 12
3.7. Perovskite Materials ... 13
3.8. Many-Particle Problem ... 13
3.8.1. Born-Oppenheimer approximation ... 14
3.8.2. Hartree method and self-consistent field method ... 15
3.8.3. Hartree-Fock method, Slater determinant and exchange energy ... 15
3.9. Thomas-Fermi Theory and Dirac Change Energy ... 17
3.10. Density Functional Theory (DFT) ... 17
3.10.1. Hohenberg-Kohn's Theorem ... 18
3.10.2. Kohn-Sham Equation ... 18
3.11. Local density approximation (LDA) ... 19
3.12. Generalized Gradient Approach (GGA) ... 20
3.13. Pseudo-Potential Method ... 20
3.14. Elastic Properties of the Solids ... 20
4. RESULTS AND DISSCUSION ... 25
4.1. Some Properties of $BaIrO_3$ Crystal ... 25
4.2. Structural Properties of $BaIrO_3$ Crystal ... 25
4.2.1. Cut-off energy ... 26
4.2.2. Number of k-points ... 27
4.2.3. Volume optimization ... 31
4.2.4. Lattice parameters of $BaIrO_3$ crystal ... 35
4.2.5. Unit cell and bond lenghts of $BaIrO_3$ crystal ... 36
4.3. The Electronic Properties of $BaIrO_3$ Crystal ... 39
Page

4.3.1. Electronic band structure 39
4.3.2. Density of states (DOS) 41
4.3.3. Partial density of states (PDOS) 42
4.4. The Elastic Properties of $BaIrO_3$ Crystal 49
5. CONCLUSION 53
REFERENCES 55
EXTENDED TURKISH SUMMARY 59
CURRICULUM VITAE 71

LIST OF TABLES

Table **Page**

Table 3.1. matrix representation and tensor representation. 21
Table 4.1. The calculated lattice parameter, volume and total energy values of $BaIrO_3$ crystal…………………..…………………………………………….36
Table 4.2. Bonds and the bond lengths in $BaIrO_3$ crystal. 37
Table 4.3. The atomic coordinates and the Wcykoff positions of the atoms in the $BaIrO_3$ crystal. 37
Table 4.4. The cartesian coordinates of the Γ-X-M-R high symmetry points in the first Brillouin zone. 39
Table 4.5. The calculated elastic stiffness constants of $BaIrO_3$ crystal under GGA and LDA approximations. 49
Table 4.6. The calculated elastic compliance constants of $BaIrO_3$ crystal under GGA and LDA approximations. 49
Table 4.7. Some elastic modulus and constants of $BaIrO_3$ crystal under GGA ve LDA approximations. 51

x

LIST OF FIGURES

Figure **Page**

Figure 3.1.The Fundamental Types of Crystalline Solids 6

Figure 3.2. Crystal lattice and unit cell.. 6

Figure 3.3. One dimensional crystal lattice 7

Figure 3. 4 Bravais lattices in two dimensional lattice 8

Figure 3. 5. Crystal systems in three dimentional lattice... 9

Figure 3.6 Bragg’s law (Jauncey, 1924) 10

Figure 3.7 Brillouin zones 11

Figure 4.1. The total energy versus cut-off energy graph for $BaIrO_3$ crystal under GGA……………………………………………………………………….27

Figure 4.2. The total energy versus cut-off energy graph for $BaIrO_3$ crystal under LDA ……….……………………………………………………………….……28

Figure 4.3. Total energy vs. Monkhorst-Pack Grid graph of $BaIrO_3$ crystal under GGA………………………………………………………………………..29

Figure 4.4. Total energy vs. number of k-points graph of $BaIrO_3$ crystal under GGA……….30

Figure 4.5. Total energy vs. Monkhorst-Pack Grid graph of $BaIrO_3$ crystal under LDA……………………………………………...…………………30

Figure 4.6. Total energy vs. number of k-points graph of $BaIrO_3$ crystal under LDA...31

Figure 4.7. Total energy vs. volume graph of $BaIrO_3$ crystal under GGA…………….32

Figure 4.8. Total energy vs. volume graph of $BaIrO_3$ crystal under LDA. 33

Figure 4.9 Total energy vs. pressure graph of $BaIrO_3$ crystal under GGA 33

Figure 4.10. Total energy vs. pressure graph of $BaIrO_3$ crystal under LDA 33

Figure 4.11. Pressure vs. volume graph of $BaIrO_3$ crystal under GGA 34

Figure 4.12 Pressure vs. volume graph of $BaIrO_3$ crystal under LDA 34

Figure 4.13. Total energy vs. lattice parameter graph of $BaIrO_3$ crystal under GGA. ... 35

Page

Figure 4.14 Total energy vs. lattice parameter graph of $BaIrO_3$ crystal under LDA. 36

Figure 4.15. The unit cell of the $BaIrO_3$ crystal obtained by Vesta with two different point of views (Momma & Izumi, 2011) 38

Figure 4.16 Electronic band structure of $BaIrO_3$ under GGA. The Fermi energy level is given with red horizontal line 40

Figure 4.17 Electronic band structure of $BaIrO_3$ under LDA. The Fermi energy level is given with red horizontal line 40

Figure 4.18. Density of states graph of $BaIrO_3$ crystal under GGA. The vertical red line shows the Fermi energy level 41

Figure 4.19. Density of states graph of $BaIrO_3$ crystal under LDA. The vertical red line shows the Fermi energy level 42

Figure 4.20. The partial density of states (PDOS) graph of Ba atom under GGA 43

Figure 4.21. The partial density of states (PDOS) graph of Ir atom under GGA 44

Figure 4.22. The partial density of states (PDOS) graph of O(1) atom under GGA 44

Figure 4.23. The partial density of states (PDOS) graph of O(2) atom under GGA 45

Figure 4.24. The partial density of states (PDOS) graph of O(3) atom under GGA 46

Figure 4.25. The partial density of states (PDOS) graph of Ba atom under LDA. 46

Figure4.26. The partial density of states (PDOS) graph of Ir atom under LDA 47

Figure 4.27. The partial density of states (PDOS) graph of O(1) atom under LDA. 47

Figure 4.28. The partial density of states (PDOS) graph of O(2) atom under LDA. 48

Figure 4.29. The partial density of states (PDOS) graph of O(3) atom under LDA. 48

SYMBOLS AND ABBREVIATIONS

Some symbols and abbreviations used in this study are presented below, along with descriptions.

Symbols	**Description**
ABINIT	Program using pseudo-potential method based on density functional theory
Ba	Barium
BaIro$_3$	Barium iridate
C_{ij}	Elastic stiffness constant
DFT	Density functional theory
DOS	Density of states
E_{cut}	Cut-off energy
E_f	Fermi energy
E_g	Energy Gap
E_{HF}	Hartree-Fock energy
E_0	Ground state energy
Ir	Iron
LDA	Local density approximation
O_3	Ozone
GGA	General gradient approximation

1. INTRODUCTION

Indeed, energy generation and storage are the two significant problems of all time. In this century, scientists are invited new functional materials that they are powerful in energy power generation and storage. Due to their low cost, availability in nature and less environmental impact, sunlight is one of the quit significant infinite sources of energy (Zhang et al., 2016). According to physical properties and structural materials, perovskites are unique in photovoltaic applications, which this feature is important for solar cell devices (Stoumpos and Kanatzidis, 2016).

The classes of perovskites adopt the chemical formula as ABX_3, where A is a monovalent cation (e.g., Cs^+, Rb^+ …), B is a bivalent metal cation (e.g., Pb^{+2}, Sn^{+2} or Ge^{+2}) and X is a halide anion (e.g Cl^-, Br^-, I^-). When X=O (oxygen) then it is called oxide perovskites, when X= inorganic halide (I, Cl, Br) it is called halide perovskites and the other subgroup is hybrid organic-inorganic halide perovskite, generally denoted as $CH_3NH_3PbI_3$ ($MAPbI_3$) (Chen et al., 2015).

The magnetic and electronic characteristics of transition-metal oxides are being widely investigated during the last several years (Cheng et al., 2009). The materials which exhibit ABO_3 peroviskite form are important class, because they are important in a variety of device application area. These are the materials used for particular ceramic capacitors. Piezoelectric PLZT ceramic discs made from ABO a type oxide is well known for their use in a variety of transducer devices such as phonograph pick-ups, strain gauges, ultrasonic equipment etc.

Metal hybrid perovskites have been extensively studied for solar cells, photodetectors, lasing, light-emitting diodes, etc., owing mainly to their excellent semiconductor properties, low cost, low trap-state densities and long carrier diffusion lengths, direct band gap, relatively have high light absorption coefficients, high carrier mobility, adjustable spectral absorption ranges and band gap, long charge diffusion lengths, intense photoluminescence, low rates of non-radiative charge recombination superior charge transfer properties.

Barium iridate, $BaIrO_3$, has recently attracted a lot of attention due to the discovery of the development of charge -density-wave (CDW) and weak ferromagnetism at the same temperature at 180°C. This is the first recognized ferromagnet to possess 5d metal transition cation in ternary oxide. The crystalline structure of $BaIrO_3$ is cubic (space group $Pm\bar{3}m$).

The aimed of this study is to investigate some physical properties of $BaIrO_3$ peroskite prystal with Density Functional Theory within the generalized gradient approximation (GGA) and the local density approximation (LDA). Structural, Electronic and Elastic features of $BaIrO_3$ had been reported. using the ABINIT software programe.

2. LITERATURE REVIEW

In recent years, many researchers where successful in calculating electronic, elastic, thermodynamical, mechanical and electrical properties of materials using density functional theory, this method is an effective way to predict material properties before synthesis in laboratory.

During literature review it is revealed that only small amount of researches to study $BaIrO_3$ were performed and the detail was not given. J.G. Cheng et al. had been practically synthesis $BaIrO_3$ under the high-pressure sequence by means of solid-state reaction and slow cooling in air to yield an almost fully oxygen-stoichiometric, after fabrication they analyzed its properties by carried out XRD under each different value of temperature they reported that four phases have been identified, the so-called "9R", 5H, 6H, and 3C structures (Cheng et al., 2009).

M. A. Laguna-Marco and their team concentrated to study the role of orbital magnetism and spin-orbit on electronic structure of $BaIrO_3$ this aim was examined by x-ray absorption techniques, far away from predictions they conclude that the Ir 5d orbital moment approximately 1.5 times greater than the spin moment according to their study orbital interactions can not be neglected when addressing the nature of magnetic ordering in $BaIrO_3$ (Marco et al., 2010).

J. Zhao et al. reported about structure and physical properties of the 6M $BaIrO_3$, distorted hexagonal fabricated under high temperature sintering. From XRD analysis lattice parameters are defined and the average Ir-O distance and direct Ir-Ir distance determined as 2.067(19) and 2.719(1) Å, respectively, and it is not obey the Fermi liquid behavior also Both magnetic susceptibility and specific heat data show that it is an exchange-enhanced Pauli paramagnet, because of the electron-electron correlation effect (Zhao et al., 2009).

As considered above the physical properties of $BaIrO_3$ material are still under investigation and are not revealed at all, also the number of studies on the material is limited. Also all those previous studies are experimental. According to our knowledge there is no theoretical study on physical properties of $BaIrO_3$ cubic crystal in the literature. Except for the studies given above, there is a literature about $BaIrO_3$, that we have taken the lattice parameter valur, which is the “Materials Project” web page. In this web page, scientists reveal their studies about many materials, but those results are not all the time tested, and reliable. We just taken a starting value for the lattice parameter but we also theoretically computed the lattice parameter that we use in this computational study. In this thesis $BaIrO_3$ is chosen to investigate the physical properties of this material with the help of density functional theory by using ABINIT software program. The novelty of this thesis comes from the fact that there are no researches up to now to explain property of this material in detail and it may consider a big contribution in literature.

3. THEORETICAL BACKGROUND

In this part of the study, all relevant and necessary theoretical information is explained in detail such as the crystal structure, unit cell, primitive translation in the bravais lattice and reciprocal lattice vectors, spacing between planes in crystals, band structure and the elastic properties of the crystals.

The calculation method depends on the Density Functional Theory which is also explained here starting from the very beginning of the many body problems, in detail. The historical development up to Density Functional Theory is given with all important approaches.

3.1. Classification of Solids and Crystal Structure

The classifying of solids can be according to type of atomic ordering, bond between atoms, chemical or physical features of solid or geometrical elements of the crystalline shape (Li, 2006). If the arrangement of the atoms does not obey any specific long or short ordering known as amorphous solids, in the other hand the atoms which have regular arrangement called crystal. Also the crystalline solids classify into two categories: single crystalline and polycrystalline, in single crystalline structure solids have a regular atomic ordering across whole of the crystal, where the polycrystalline solids are the same as single crystalline the only difference that polycrystalline solids have a specific regular arrangement atoms only in the small parts of crystalline can be due to many reasons such as vacant positions , impurity, out of location and existence grain surrounding(Park et al., 2017) . The solids also grouped based on their electrical conductivity into conductors, semiconductors and insulator.

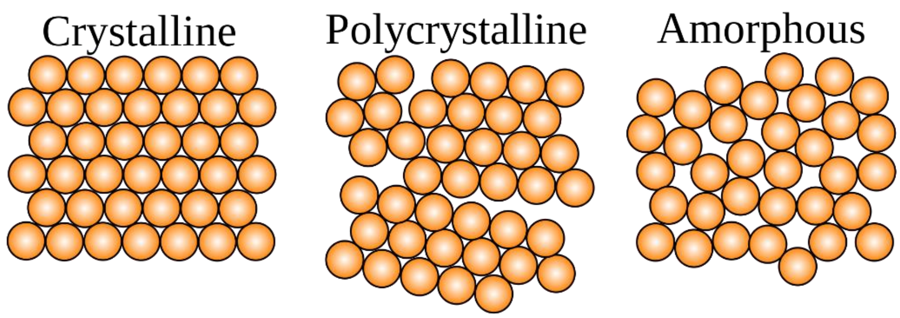

Figure 3.1. The fundamental types of crystalline solids.

3.1.1. Crystal structure

The smallest regular part of crystalline that repeated sequently over three dimensional crystal known as unit cell as shown in Figure 3.2.

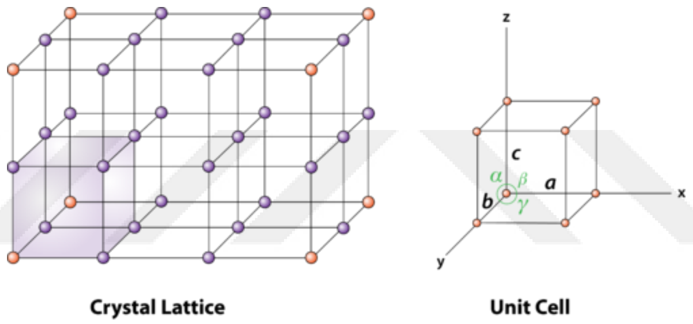

Figure 3.2. Crystal lattice and unit cell.

Basically every crystal made up from summation of lattice points and basis together and it can simply expressed as follow (Gavezzotti, 2011),

Crystal = lattice + basis

Lattice can be defined as a group of points, that ordered in regular array so that neighbored of each point in the lattice are the same where the basis is consist of one or more than one atoms that arranged in special way regarding to other atoms. The crystal structures, is made as result of the certain arrangement of atoms.

1.1.3. Types of crystal lattice

Based on repetition of crystal lattices along x,y and z axis the crystals are divided into three types: one, two and three dimensional crystal structure categories. The result of those arrangements leads to form different kinds of crystal structures. In the following sections the one, two and three dimentional lattice structures will be explained briefly.

1.1.4. One dimensional crystal

The simplest crystal is one dimensional crystal lattice. In this type of lattice if the number of atoms is N, then all atoms are arranged on the same path with equally space distance together or periodically repeated.

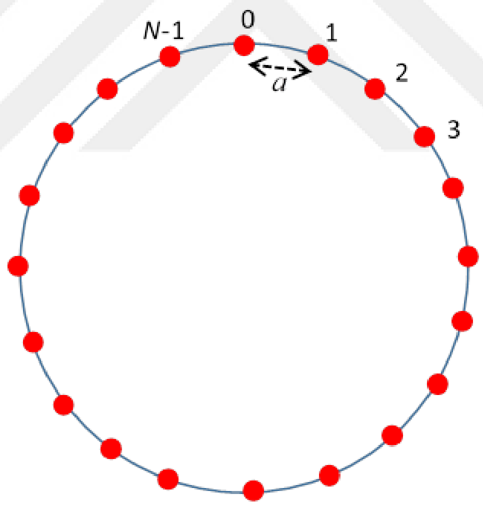

Figure 3.3. One dimensional crystal lattice.

This arrangement can be either like a circle as given in Figure 3.3, or it can be as a linear line. In one dimensional crystal lattice, a refers to the lattice constant and N represent the number of atoms. The main feature of this kind crystal lattice has translation symmetry property in the both structure and internal arrangement.

1.1.5. Two dimensional crystal

The simple two-dimensional crystal lattice consist one or more than one kind of atoms which have two coordinate axis (i.e two independent basis vector) the angle between them is γ (Raj et al., 2008).

In 2-D lattice, there are five different Bravais lattices. Those are, Oblique, Rectangular primitive, Rectangular centered, Hexagonal and Square. As shown in Figure 3.4.

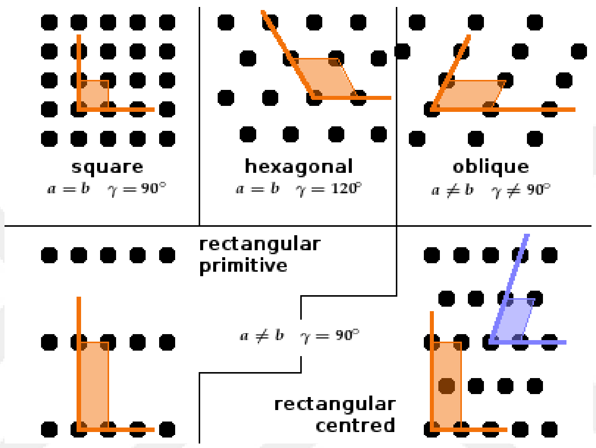

Figure 3. 4. Bravais lattices in two dimensional lattice.

The lattice is expressed by translation vectors. For example, the position vector of any two dimensional lattice in Figure 3.4 can be expressed as below:

$$\tau = n_1\boldsymbol{a} + n_2\boldsymbol{b} \tag{3.1}$$

where **a** and **b** are vectors that indicated in Figure 3.4 and n_1,n_2 are integer values depend on lattice position.

1.1.6. Three dimensional crystal

There are fourteen different three-dimensional lattices which are called Bravais lattice and divided into 7 crystal systems. Each crystal system depends on the shape of the unit cell and according to its symmetry (Ghosh, 2005). Additionally there are three vectors (i.e lattice parameters) known as a, b and c with three angles α, β *and* γ. The unit cells are divided into three classes according to the positions of the additional atoms, such as, side centered, body-centered and face centered. If there is no additional atom in a unit cell, then it is called primitive unit cell.

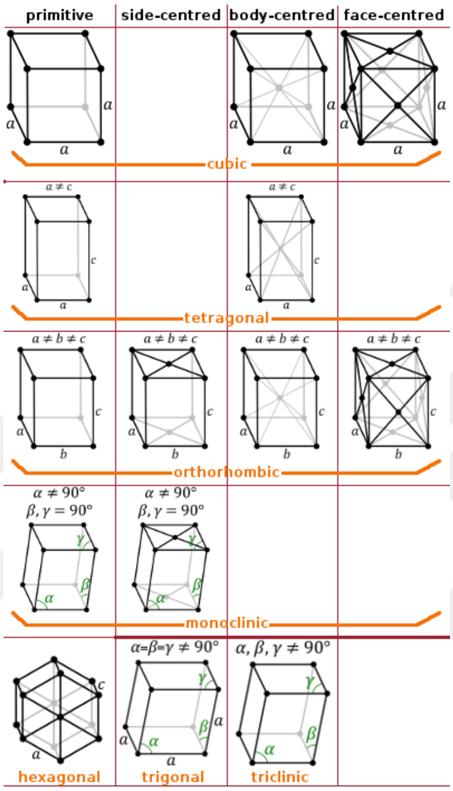

Figure 3.5. Crystal systems in three dimentional lattice.

In the Figure 3.5 the seven crystal structures and the crystal lattices for the three dimentional crystal is given.

3.2. Diffraction in Crystals and Bragg's Law

If the space between atoms close to (i.e comparable with) the wavelength of x-ray around 1A^{o} then the diffraction pattern can be observed in crystals (C.Kittel, 2005; Humphreys, 2013). Also, the crystal structure can be investigated using electron and neutron diffraction (Babilas et al., 2020). If we consider only to rows of the atoms with interatomic distance d, and exposed by x-ray with wavelength equal to λ and incident angle is θ, then the first ray will be reflected from the surface (first layer) and the second ray will be reflected from the next layer then the constructive interface will occur only if over all path of the two reflected waves equal to integer number of x-ray wavelength $n\lambda$ as shown in Figure 3.6 . This known as Bragg's law and mathematically can be expressed as bellow (Kacher et al., 2009):

$$2d sin\theta = n\lambda \tag{3.2}$$

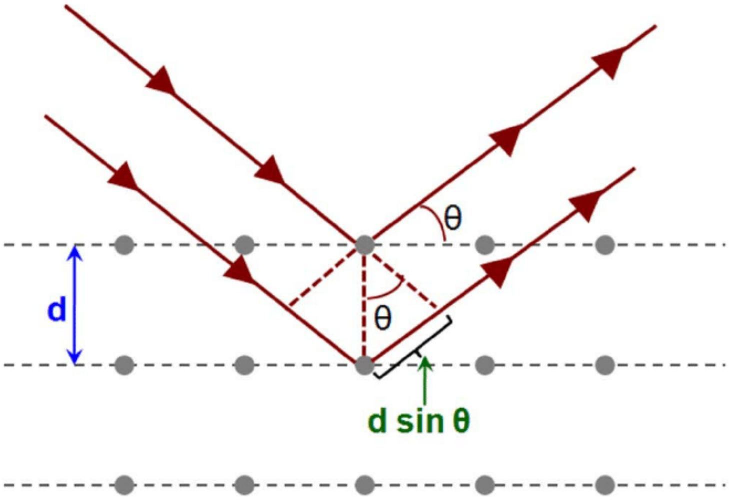

Figure 3.4. Bragg's law (Jauncey, 1924).

3.3. Reciprocal Lattice

The concept of reciprocal lattice has a great advantage in studying the structural , optical and electrical properties of solids (Bown & Gay, 1959). Reciprocal lattice vectors consist three primitive vectors which symbolized by $\overrightarrow{b_1}, \overrightarrow{b_2}$ *and* $\overrightarrow{b_3}$. And each of them can be determine by taking the reciprocal of real lattice vectors. Any crystal structure has its own reciprocal lattice vector and during performing any experiment it is play as identifier role. The reciprocal lattice vector can be expressed as below (C.Kittel, 2005):

$$\vec{G} = n_1'\overrightarrow{b_1} + n_2'\overrightarrow{b_2} + n_3'\overrightarrow{b_3} \tag{3.3}$$

where n_1', n_2' *and* n_3' are integers. The reciprocal lattice vectors can be found with respect to real space lattice by applying following equations (Ebalard and Spaepen, 1989):

$$\overrightarrow{b_1} = 2\pi \frac{(\vec{b}\mathrm{x}\,\vec{c})}{\vec{a}(\vec{b}\mathrm{x}\,\vec{c})} \tag{3.4}$$

$$\overrightarrow{b_2} = 2\pi \frac{(\vec{c}x\,\vec{a})}{\vec{a}(\vec{b}x\,\vec{c})} \tag{3.5}$$

$$\overrightarrow{b_3} = 2\pi \frac{(\vec{a}x\,\vec{b})}{\vec{a}(\vec{b}x\,\vec{c})} \tag{3.6}$$

Every lattice vectors that expressed in above equation make an angle which equal to 90^0 with two other vectors in real space. Therefore, reciprocal lattice vectors obey following relationship (Humphreys, 2013):

$$\overrightarrow{b_\iota}.\overrightarrow{a_j} = 2\pi\delta_{ij} \tag{3.7}$$

In other words, the multiplication of the real and the reciprocal lattice of same directions gives 2π , but the multiplication of different directions gives zero.

3.4. Brillouin Zone

The unit cell with the lowest volume in real space is known as Wigner-Seitz cell and as first brilluoin zone in k-space as shown in Figure 3.7. Formed via drawing perpendicular reciprocal lattice vectors from the center to the nearest reciprocal point cell and by intersecting planes. It is significant because it permits to choose any wanted shape to reciprocal lattice vector. Because of symmetry property the electronic wave function is similar for all k points (Barr, Barr, Porter, & Reichl, 2017).

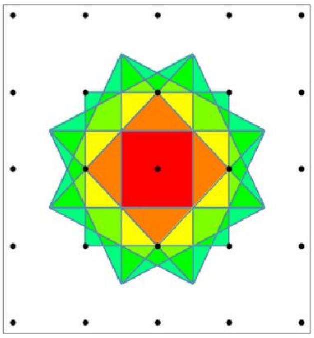

Figure 3.7. A series of brillouin zopnes.

In Figure 3.7, the red square is the first Brillouin zone, the orange square is the second Brilluoin zone and so on.

3.5. Electronic Band Structure in Crystals

The conductivity property of materials such as conductor, semiconductor or insulator is determined by band structure which is the key of understanding conductivity. It is well known that every single atom in crystals have interaction with other surrounding atoms. According to coulomb's law opposite electric charges are attract each other and same electric charges are repelled each other. These two forces are inversely proportional with square of the distance between them (Gorelov et al., 2020).

When two atoms close together, both interactions occur due to their outer shell electrons and positive nuclei. I the number of atoms increase, it is obvious that each atom interact with that atom in different force due difference the square distance from that atom. As result of all these interactions, infinite continuous energy levels are created; they are overleaped and becomes undistinguishable. They start from lower energy to the higher energy (Tancogne et al., 2017).

The fulfilled electron bands are called valance band, where empty or partially fulfilled bands are known as conduction band. The space between these two bands is called energy gap (E_g), the possibility of existence electron in energy gap is zero.

In conductors both valance band and conduction band are overleaped (i.e energy gap is zero), and for semiconductors energy band range typically between 1-3 eV, for the higher band gap values, then the material can be considered as an insulator.

3.6. Density of States (DOS)

Density of state basically is the quantity of various states at a certain energy level that electrons are permitted to stay in. It gives information about either the material is conductor, semiconductor or insulator. Generally, density of state refers to the available states to electron take place and show how the energy levels close together. Mathematically expressed as below (Alexander & Orbach, 1982):

$$D(\omega) = \frac{dN}{dE} \tag{3.8}$$

where $D(\omega)$, N and E are density of states, number of electrons and energy, respectively.

3.7. Perovskite Materials

This kind of mineral was found by the U. Mountains of Russia by Gustav Rose in 1839. They made up from molecules and represented by ABO_3 which A refer to the largest radius ion and is located at the center of lattice, B is smallest radius ion and is located at the corners of lattice and O is oxygen. Their main distinguishable features are stability, cheapness, most efficient in converting light to electric energy that is why they are used in solar cells. Additionally, they can be developed in laboratory to increase their efficiency. Some known perovskites are $CaTiO_3$, $BatiO_3$, $PbTiO_3$ and $KNbO_3$ in this study $BaIrO_3$ is used as a perovskite material (Heo et al., 2020).

3.8. Many-Particle Problem

When two or more different atoms combine and bind together, they form molecules and solids which consist a large number of molecules and they interact with each other in many different ways. There is no expression to describe such kind of complex system. It is needed to solve time-independent Schrödinger equation which is given by (Bornath et al., 1999):

$$\hat{H}\psi = E\psi \tag{3.9}$$

where $\hat{H}$ is the Hamiltonian operator, E is the energy and ψ is wave function. Hamiltonian with its individual elements can be expressed as following (Lovett et al., 2013):

$$\hat{H} = \hat{T}_e + \hat{T}_i + \hat{V}_{ii} + \hat{V}_{ee} + \hat{V}_{ie} + \hat{V}_{ext} \tag{3.10}$$

where $\hat{T}_e$ is the kinetic energy of electrons, $\hat{T}_i$ is the kinetic energy of the ion, $\hat{V}_{ii}$ is the ion-ion interaction potential energy, $\hat{V}_{ie}$ is the ion-electron interaction potential energy, $\hat{V}_{ee}$ is the electron-electron interaction potential energy and $\hat{V}_{ext}$ is the external applied potential energy. It is obvious from above equation that it is diificult or even impossible to solve it directly. It requires simplification, so some approximations should be applied.

The Eq. 3.10 can be written as follows with an assumption as $m_i = m_e = e = \hbar = 1$,

$$\hat{H} = -\frac{1}{2}\sum_{i=1}^{N}\nabla_i^2 - \frac{1}{2}\sum_{j=1}^{M}\nabla_j^2 + \frac{1}{2}\sum_{i\neq j}^{N}\frac{1}{|\vec{r_i} - \vec{r_j}|} + \frac{1}{2}\sum_{\alpha\neq\beta}^{M}\frac{Z_\alpha Z_\beta}{|\overrightarrow{R_\alpha} - \overrightarrow{R_\beta}|} - \frac{1}{2}\sum_{i=1}^{N}\sum_{\alpha=1}^{M}\frac{Z_\alpha}{|\vec{r_i} - \overrightarrow{R_\alpha}|} + \widehat{V_{ext}}(\vec{r_1}, \vec{r_2}, \ldots, \vec{r_N}, \overrightarrow{R_1}, \overrightarrow{R_2}, \ldots, \overrightarrow{R_M}) \quad (3.11)$$

For a system that contains one electron, it is easy to solve the Schrödinger equation, but every real systems consist of a huge number of electrons therefore it is impossible to solve it, so approximations are necessary.

3.8.1. Born-Oppenheimer approximation

According to Born-Oppenheimer approximation electrons are much faster than ions due to their very light masses. In such situation ions can be assumed almost stationary relative to the electrons. Therefore kinetic energy of the ions could be neglected while compared with kinetic energy of electrons in Equation 3.11 and the distance between ions remain the same, so ion-ion potential interaction can be consider as a constant. By rewriting Equation 3.11 based on this approximation and assuming external potential is zero, then it is expressed (Combe et al., 1981):

$$\hat{H} = \hat{T}_e + \hat{V}_{ee} + \hat{V}_{ei} = -\frac{1}{2}\sum_{i=1}^{N}\nabla_i^2 + \frac{1}{2}\sum_{i\neq j}^{N}\frac{1}{|\vec{r_i} - \vec{r_j}|} - \frac{1}{2}\sum_{i=1}^{N}\sum_{\alpha=1}^{M}\frac{Z_\alpha}{|\vec{r_i} - \overrightarrow{R_\alpha}|} \quad (3.12)$$

All terms of Eq. 3.12 are written according to electrons. Even it is still difficult to solve due to too much electron-electron interactions, also above equation is useless while electrons and nuclei are not in relative motion together. This approximation was improved by Hartree afterwards.

3.8.2. Hartree method and self-consistent field method

Hartree supposed that there is a mean field for interacting electrons. According to this assumption, electrons interact with the mean field equally with other electrons and ions. By this mean electron-electron interaction can be considered as zero in Eq. 3.12 and multi-electron Schrödinger equation converts to single-electron schrodinger equation. If N is total number of electrons then N-1 electrons generate a cloud of mean potential. Here Schrodinger equation for single-electron wave function is used. The total wave function can be found by multiplying all wave functions together and total energy of the system is equal to the sum of every single electron's energy as shown below(Slater, 1953):

$$\psi_e(\vec{r}_1, \vec{r}_2, \ldots, \vec{r}_N) = \prod_{i=1}^{N} \psi_i(\vec{r}_1) \tag{3.13}$$

$$E_e = \sum_{i=1}^{N} E_i \tag{3.14}$$

The final Hartree expression for single electron can be written as following (Thogersen et al., 2004):

$$-\frac{1}{2}\nabla_i^2\, \psi_i(\vec{r}_i) + \left[\frac{1}{2}\ \sum_{j\neq i} \int \left|\psi_i(\vec{r}_j)\right|^2 \frac{d\,\vec{r}_j}{|\vec{r}_i - \vec{r}_j|}\right] \psi_i(\vec{r}_i) - U_i(\vec{r}_i)\psi_i(\vec{r}_i) = E_i\psi_i(\vec{r}_i) \tag{3.15}$$

In this approximation there are some important mistakes. Firstly, exchange energy between electrons is not taken into account. Secondly Hartree approximation does not obey Pauli principle, because the electronic wave function is written as the product of the wave functions of individual electrons and remains symmetrical with the displacement of any two electrons.

3.8.3. Hartree-Fock method, Slater determinant and exchange energy

In Hartree-fock method electron wave function is expressed as anti-symmetric multiplying of electron orbitals. That is very close to the real situation that electrons are anti-symmetric as shown (Della and Gorling, 2001):

$$\psi(\vec{r}_1, \vec{r}_2, \dots, \vec{r}_N) =$$
$$\frac{1}{\sqrt{N!}}[\psi_1(\vec{r}_1 s_1)\psi_2(\vec{r}_2 s_2) \dots \psi_N(\vec{r}_N s_N) - \psi_1(\vec{r}_2 s_2)\psi_2(\vec{r}_1 s_1) \dots \psi_N(\vec{r}_N s_N) + ..]$$
(3.16)

The Equation 3.16 obeys Pauli exclusion principle. Slater wrote this expression as a deyterminant with size N×N as following (Sahni, 1997):

$$\psi(\vec{r}_1\vec{s}_1, \vec{r}_2\vec{s}_2 \dots \vec{r}_N\vec{s}_N) = \frac{1}{\sqrt{N!}} \begin{vmatrix} \psi_1(\vec{r}_1 s_1) & \psi_1(\vec{r}_2 s_2) & \dots & \psi_1(\vec{r}_N s_N) \\ \psi_2(\vec{r}_1 s_1) & \psi_2(\vec{r}_2 s_2) & \dots & \psi_2(\vec{r}_N s_N) \\ . & . & & . \\ . & . & & . \\ . & . & & . \\ . & . & & . \\ . & . & & . \\ \psi_N(\vec{r}_1 s_1) & \psi_N(\vec{r}_2 s_2) & \dots & \psi_N(\vec{r}_N s_N) \end{vmatrix} \quad (3.17)$$

The predicted value of energy could be determined using above wave function equation and latest Hamiltonian function. Hartree-fock is a general part of Hartree equation, the main difference is that the Hartree-fock summarized by smallest energy as expressed below (Amusia et al., 2003; Gorling and Levy, 1997):

$$-\frac{\hbar^2}{2m_e}\nabla_i^{\,2}\, \psi_i(\vec{r}_i) \left[\frac{1}{2}\ \sum_{j\neq i} \int \left| \psi_i(\vec{r}_j)\right|^2 \frac{e^2 d\,\vec{r}_j}{4\pi\varepsilon_0 |\vec{r}_i - \vec{r}_j|}\right] \psi_i(\vec{r}_i) + U_i(\vec{r}_i)\psi_i(\vec{r}_i)$$
$$- \sum_j \int \frac{e^2 d\vec{r}_i d\vec{r}_j}{|\vec{r}_i - \vec{r}_j|} \psi_j^{\,*}(\vec{r}')\psi_i(\vec{r}')\psi_j(\vec{r})\delta_{s_i s_j} = E_i\psi_i(\vec{r}_i) \quad (3.18)$$

The last part in above equation is the exchange energy, and it is noticed that this equation is free from any weak points. The wave function yielded from Hartree-fock equation is special for independent electron systems, even the electrons interact in real system. The interaction energy which is not exist in the Hartree-Fock theory is called correlation energy. Correlation energy is defined as the difference between the energy in the Hartree-Fock limit (EHF) and the exact non-relativistic energy of a system, expressed as below (Amusia et al., 2003) :

$$E_C = E_0 - E_{HF} \quad (3.19)$$

Where E_C is correlation energy, E_o is total energy and E_{HF} is Hartree-fock energy.

3.9. Thomas-Fermi Theory and Dirac Change Energy

This theory postulated by Thomas and improved by Dirac. It is the simplest theory that explains electronic structure of atoms and molecules using density of electrons. This theory state that electron density is main value and plays important role. Therefore, the electron wave function replaced by electron density. In this theory Hamiltonian composed by electron density not electron wave function (Cowan and Ashkin, 1957). By this method total energy can be determined. The main features that make this theory more significant are: electrons mannered as independent particles and both correlation energy and exchange energy are ignored.

3.10. Density Functional Theory (DFT)

Density functional theory is a method that can find solution for multi-particle problem. Hohenberg and Kohn introduced density functional theory based on thomas-dirac theory. Density functional theory is a powerful method to describe the atomic structure of solids, atoms and molecules. Density functional theory use electron density as a fundamental for its calculation while other approximations used wave function instead. Getting solution via electron density is easier than utilizing wave function because the degree of freedom for electron density is one where wave function has three degree of freedoms. That explains why it is very suitable to use electron density as a basic variable (Geerlings et al., 2003).

Using quantum mechanics laws, density functional theory capable to explain ground state properties of metals, insulators and semiconductors. Also, this theory is powerful in measuring physical material properties such as optic, elastic, volume, band structure, etc. In this theory, Kohn-Sham equations are solved instead of Schrödinger equations.

3.9.1. Hohenberg-Kohn's theorem

According to this theorem, the ground-state energy from Schrödinger's equation is a unique functional of the electron density. There are two important theorems to consider that developed by Hohenberg and Kohn as follow:

The first Hohenberg–Kohn theorem states that the ground state of any interacting many particle system with a given fixed inter-particle interaction is a unique functional of the electron density n(r) (Epstein and Rosenthal, 1976).

The second Hohenberg–Kohn theorem defines an important property of the functional and states, which the electron density that minimizes the energy of the overall functional is the true electron density corresponding to the full solutions of the Schrödinger equation.

3.9.2. Kohn-Sham equation

Kohn-shame equation is similar as the single-electron schrodinger equation in Hartree-fock equation, but in Kohn-Sham equation there is an imaginary system that electrons are independent and non-interacting together, at the same time non-interacted electrons make the same density that by interacted electrons generate. Electrons are moved at an effective potential known as a single-particle potential.

Density functional theory tries to investigate many electron systems by using electron density as a main variable in ground state of material and ignore electron wavefunction (Bauernschmitt and Ahlrichs, 1996):

$$n(\vec{r}) = \sum_{i=1}^{N} |\varphi_i(\vec{r})|^2 \tag{3.20}$$

Also can be expressed as (Seidl, Görling, Vogl, Majewski, & Levy, 1996):

$$\left[-\frac{\hbar}{2m}\nabla^2 + V(\vec{r}) + \frac{e^2}{4\pi\varepsilon_0\varepsilon_r}\int \frac{n(\vec{r}')}{|\vec{r}-\vec{r}'|} d^3\,\vec{r}' + V_{xc}(\vec{r})\right]\phi_i(\vec{r}) = \varepsilon_i\phi_i(\vec{r}) \tag{3.21}$$

It is obvious that third term is exchange and correlation potential similar as in Hartee equation and expressed as below:

$$V_{xc}(\vec{r}) = \frac{\delta E_{xc}[n]}{\delta n(\vec{r})} \tag{3.22}$$

In order to solve the Kohn-Sham equation we have to do the following:

1- A beginning value of electron density, n(**r**) should be chosen.

2- By solving the Kohn-Sham equation a wave function for a single electron $\psi_i(\mathbf{r})$, should be determined.

3- With respect to that wave function, we g-have to determine the electron density for a single electron ($n_{KS}(r) = 2\sum_i \psi_i^*(r)\psi_i(r)$).

4- Then we have to compare the calculated electron density, $n_{KS}(\mathbf{r})$, with the electron density used in solving the Kohn–Sham equations, $n(\mathbf{r})$. If the two densities are the same, then this is the ground-state electron density, and it can be used to compute the total energy. If not, all those previous steps should be reperated. That is why, this procedure is an iterative solution (Castro et al., 2004).

As mentioned above the terms of exchange and correlation energy are excluded from Kohn–Sham equations. Therefore some approximations are performed to find the solution. Such as Generalized Gradient Approximation (GGA) and the Local Density Approximation (LDA) which are widely used to find the solution. In this thesis in order to compute the physical properties of $BaIrO_3$ perovskite crystal both approximations are used.

3.11. Local density approximation (LDA)

It postulates that the changing density of electrons over area is almost constant, and local density can be imagining as uniform electron gas. Local density functional is given by (Yabana and Bertsch, 1996):

$$E_{XC}^{LDA}[n] = \int n(\vec{r})\varepsilon_{XC}(n)d\vec{r} \tag{3.23}$$

It is clear from above equation the local density approximation is only a function of electron density. In local density approximation correlation-exchange energy is define as addition of correlation energy and exchange energy as below (Stampfl and Walle, 1999):

$$\varepsilon_{XC}(n) = \varepsilon_X(n) + \varepsilon_C(n) \tag{3.24}$$

3.12 Generalized gradient approach (GGA)

According to this approximation the correlation energy is a function for both electron density and its gradient and a complex function with x,y and z coordinates formed as below (Juan et al., 1995):

$$E_{XC}^{GGA}[n] = \int d^3 r f\ [n(\vec{r}), \nabla n(\vec{r})] \quad (3.25)$$

As seen from above equation density of electrons is not the same in every point of a crystal. Additionally, unlike local density approximation exchange-correlation energy is not equal to the sum of correlation energy and exchange energy (Burke et al., 1997):

$$\varepsilon_{XC}(n) \neq \varepsilon_X(n) + \varepsilon_C(n) \quad (3.26)$$

3.13. Pseudo-Potential Method

It is an approximation which provides an easier way to explain complicate systems. It is postulated by Hans Hellmann in 1934. This method tries to exchange the complexed non-valence electrons of the atom and nuclei by an effective potential, which known as pseudopotential. So it makes a replacement in Schrödinger formula. It cancels the Coulomb potential part and adds an effective potential term for the core electrons. Chemically active valence electrons are dealt with explicitly, while the core electrons are considered as 'frozen'. This method consideres the nuclei as rigid non-polarizable ion cores. It is possible to self-consistently update the pseudopotential with the chemical environment that it is embedded in, having the effect of relaxing the frozen core approximation (Khan et al., 2021).

3.14. Elastic Properties of the Solids

While the force applied to an object, this force transmitted among the atoms. As a result, this force leads to change in shape, the force that applied per unit area called stress. It is represented by rank-2 anisotropic but symmetric tensor. The objects that under effect of enough external force cause to change their shapes, the materials which have ability to return back to their original shape called elastic materials, otherwise the materials which are not capable to remove deformation known as inelastic materials. The ratio change length, volume or angle to its original shape known as strain which its rank-2 tensor and represented by ε_{ij} symbol. According to hook's law strain directly proportional with the stress and expressed as (Hill and Solids, 1963):

$$\varepsilon_{ij} = S_{ijkl}\,\sigma_{kl} \tag{3.27}$$

where S is elastic constant, an alternative way to represent hook's law is shown in below:

$$\sigma_{ij} = C_{ijkl}\,\varepsilon_{kl}\,, \quad C = \frac{1}{S} \tag{3.28}$$

Where C is elastic stiffness constant, both C and S are rank-4 tensors and each of them have 81 components. Even strain and stress tensors obey symmetry properties ($\sigma_{ij} = \sigma_{ji}\ and\ \varepsilon_{ij} = \varepsilon_{ji}$), each of them has 6 non-dependent components. To determine the solution for $\sigma_{ij}\ and\ \varepsilon_{ij}$ six equations with six variables for each equation is necessary. Therefore, the number of variables should not be exceed more than 36 independent. For that purpose matrix representation is used. Comparison between matrix representation and tensor representation is explained in below table:

Table 3.1. Matrix representation and tensor representation

Tensor Representation	11	22	33	23, 32	31, 13	12, 21
Matrix Representation	1	2	3	4	5	6

S_{ij} and C_{ij} coefficient can be write in matrix form as below:

$$\begin{bmatrix} S_{11} & S_{12} & S_{13} & S_{14} & S_{15} & S_{16} \\ S_{21} & S_{22} & S_{23} & S_{24} & S_{25} & S_{26} \\ S_{31} & S_{32} & S_{33} & S_{34} & S_{35} & S_{36} \\ S_{41} & S_{42} & S_{43} & S_{44} & S_{45} & S_{46} \\ S_{51} & S_{52} & S_{53} & S_{54} & S_{55} & S_{56} \\ S_{61} & S_{62} & S_{63} & S_{64} & S_{65} & S_{66} \end{bmatrix} \quad \text{and} \quad \begin{bmatrix} C_{11} & C_{12} & C_{13} & C_{14} & C_{15} & C_{16} \\ C_{21} & C_{22} & C_{23} & C_{24} & C_{25} & C_{26} \\ C_{31} & C_{32} & C_{33} & C_{34} & C_{35} & C_{36} \\ C_{41} & C_{42} & C_{43} & C_{44} & C_{45} & C_{46} \\ C_{51} & C_{52} & C_{53} & C_{54} & C_{55} & C_{56} \\ C_{61} & C_{62} & C_{63} & C_{64} & C_{65} & C_{66} \end{bmatrix} \tag{3.29}$$

The ability of a material to avoid change in its volume during exerted external pressure is known as bulk module. It can be calculated using both Voigt model and

Reuss model. The Hill model estimates an arithmetic average of the Voigt and Reuss models:

$$9B_V = (C_{11} + C_{22} + C_{33}) + 2(C_{12} + C_{23} + C_{31}) \tag{3.30}$$

$$\frac{1}{B_R} = 9(S_{11} + S_{22} + S_{33}) + 2(S_{12} + S_{23} + S_{31}) \tag{3.31}$$

$$B_{VRH} = \frac{B_R + B_V}{2} \tag{3.32}$$

Shear stress occurs when one side of object is fixed and other side is exerted by tangential force, in such situation force is called shear force, shear module is defined by the ratio between shear stress and shear strain and calculated as below:

$$15G_V = (C_{11} + C_{22} + C_{33}) - (C_{12} + C_{23} + C_{31}) + 3(C_{44} + C_{55} + C_{66}) \tag{3.33}$$

$$\frac{15}{G_R} = 4(S_{11} + S_{22} + S_{33}) - 4(S_{12} + S_{23} + S_{31}) + 3(C_{44} + C_{55} + C_{66}) \tag{3.34}$$

$$G_{VRH} = \frac{G_R + G_V}{2} \tag{3.35}$$

As known, for cubic crystals $C_{11} = C_{22} = C_{33}$, $C_{12} = C_{23} = C_{31}$ ve $C_{44} = C_{55} = C_{66}$, therefore bulk and shear modulus expressed as below :

$$B_V = B_R = \frac{1}{2}(C_{11} + 2C_{12}) \tag{3.36}$$

$$5G_V = (C_{11} - C_{12}) + 3C_{44}\ , \quad \frac{5}{G_R} = 4(S_{11} - S_{12}) + 3C_{44} \tag{3.37}$$

Young's modulus is a measure of the ability of a material to withstand changes in length when under lengthwise tension or compression. Sometimes referred to as the modulus of elasticity, Young's modulus is equal to the longitudinal stress divided by the strain, as shown in below:

$$E = \frac{9G_{VRH}\, B_{VRH}}{G_{VRH} + 3B_{VRH}} \tag{3.38}$$

The Poisson ratio is defined as the negative ratio of transverse strain to longitudinal strain, as given:

$$v = \frac{3B_{VRH} - E}{6B_{VRH}} \tag{3.39}$$

The critical value of the Poisson ratio is 0.26 ($\cong 0.3$). If the calculated Poisson ratio of a material is bigger than this value, then this material is elastic material. But if the calculated value of Poisson ratio issmeller than this critical value, that material is said to be fragile material.

The ratio between bulk modulus to shear modulus called coefficient of elasticity. Represented by K, as shown as follows:

$$K = \frac{B_{VRH}}{G_{VRH}} \tag{3.40}$$

If the value of coefficient of elasticity greater than 1.75 then this material is flexible, but if the value smaller than 1.75 then the material considers as fragile.

4. RESULTS AND DISSCUSION

4.1. Some Properties of $BaIrO_3$ Crystal

The $BaIrO_3$ crystal has cubic and monoclinic structures. But in this study we studied on its cubic phase. In its cubic phase, $BaIrO_3$ is also a perovskite crystal. The name of $BaIrO_3$ is Barium Iridium Oxide. Space group of this crystal is $Pm\bar{3}m$ (Space group No: 221) and the Point group is $m\bar{3}m$.

In the investigation of $BaIrO_3$ crystal we calculate the lattice parameter, the total energy, the volume, pressure behaviours of $BaIrO_3$ cubic crystal in the ground state.

4.2. Structural Properties of $BaIrO_3$ Crystal

In this study we investigated the structural, electronic and elastic properties of $BaIrO_3$ crystal by using ABINIT computer programme which depends on the Density Functional Theory (DFT). We performed all these calculations under two approximations, namely, the Generalized Gradient Approximation (GGA) and the Local Density Approximation (LDA) and we compared our results. As mentioned in the previous chapter of this thesis work, ABINIT based on the pseudo-potantial method. There are some different pseudo-potential files for the atoms in each elements. In this study we used Trouller-Martins pseudo-potantials for both approximations such as GGA and LDA. In this thesis we performed all calculations by using ABINIT except for sketching the unit cell structure, calculating the bonds and bond lenghts. For those calculations we used VESTA computer programme (Momma and Izumi, 2011).

In order to investigate the structural, electronic and elastic properties of $BaIrO_3$ cubic crystal, first of all we performed cut-off energy optimization and after that we performed k-points optimization in both approximations (GGA and LDA). We decided the values of cut-off energy and number of k-points, then we used those values throughout the calculations in this thesis study. After this, we made the volume optimization in order to calculate the theoretical value of lattice parameter of $BaIrO_3$ crystal. By the volume optimization we also calculated the total energy (ground state energy) of $BaIrO_3$ crystal, the volume-total energy, pressure total energy and volume-pressure behaviours. All those results for the two approximations are given both with figures and tables.

4.2.1. Cut-off energy

The wave function of an electron can be written as a summation of discrete plane wave set for a $\vec{k}$ point as given below. This summation has infinite number of terms (Kittel, 1996).

$$\psi_{n\vec{k}}(\vec{r})=\sum_{\vec{G}} C_{n,\vec{k}+\vec{G}}\, e^{i(\vec{k}+\vec{G})\vec{r}} \tag{4.1}$$

This way of plane wave set is difficult for the most of the appications (C.Kittel, 1996). If we can finish this summation at a value before intinity, and if the result of both calculations are very close to each other, then we can get rid of those difficulties. Cutting this summation in an appropriate value makes this calculations easier and with a shorter time than before. Each plane wave sets are the values correspond to the solutions of Schrödinger equation for the kinetic energy values which is given in Eq. (4.2) (Payne et al., 1992).

$$\frac{\hbar}{2m}\left|\vec{k}+\vec{G}\right| \leq E_{cut-off} \tag{4.2}$$

The value that the summation is cutted is called cut-of energy. In order to indentify the value of cut-off energy, one can do cut-off energy optimization. In this process the programme calculates the total energy values with respect to some cut-off energy values. Afterwards a graph of total energy versus cut-off energy can be plotted. From this graph one can see that after a critical value of cut-off energy the value of total energy stays stable (see Figs. 4.1 and 4.2). The appropriate cut-off energy value should be a little bigger than this critical value but not so much bigger. If one decides a small value for the cut-off energy, then the results may be far from the real values. There may be some mistakes. Also, if one decides a very big value then the result be more close to the real one but the calculation time will be very long. So it is important to decide the appropriate value for the cut off energy.

In this study we performed the cut-off optimization for both approximations as GGA and LDA. After the optimization we plot the total energy versus cut-off energy graphs as seen in Figure 4.1 for GGA and in Figure 4.2 for LDA approximations as seen below. Both graphs are very similar to aech other. Around 816.342 eV cut-off energy value the value of total energy becomes stable. For both approximations we chosed the cut-off energy values as 1088.46 eV.

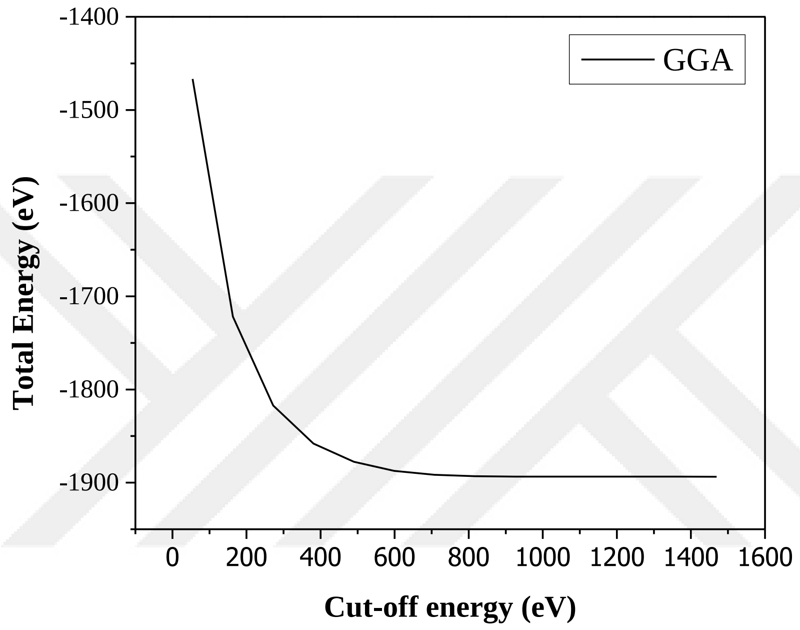

Figure 4.1. The total energy versus cut-off energy graph for $BaIrO_3$ crystal under GGA.

From Figs. 4.1 and 4.2, it is seen that the value of total energy under GGA approximation is -1893.64021 eV and it is -1896.9056 eV under LDA. It is noticed that in this optimization the results of both approximations are very close to each other.

4.2.2. Number of k-points

After calculating the cut-off energy, the next step is to calculate the number of k-points in order to be able to perform the rest of the calculations. In Density Functional Theory, the calculations are performed by taking the integrals of wave vectors over the Brillouin zone. Since there are millions of k-points, this calculation also becomes very difficult. If the calculations are performed over all k-points the process becomes too difficult, needs

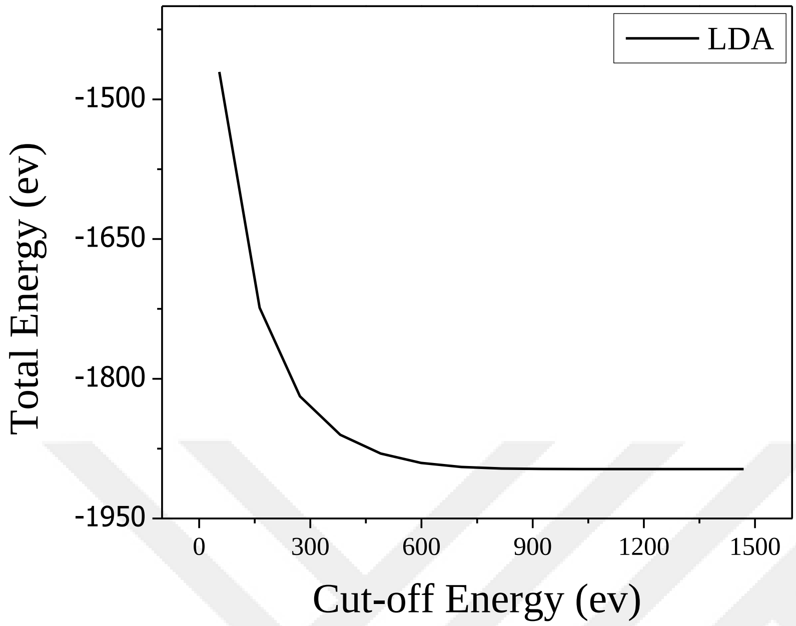

Figure 4.2. The total energy versus cut-off energy graph for $BaIrO_3$ crystal under LDA .

more capable computers and takes very long time. In order to get rid of these difficulties the symmetry properties of crystals can be used. Monkhorst ve Pack developed a method by using this symmetry properties of the crystals (Monkhorst-Pack, 1976). According to their method, they investigate some k-points which has the same symetry properties and also those has the same electronic wave function. Afterwards they only used the k-points with different electronic wave vectors. So instead of millions of k-points they used very little number of k-points. In order to investigate those k-points, the crystal is divided in to two parts along x, y and z directions. This is shown as 2x2x2 and known as 2x2x2 Monkhorst-Pack grid. For this step by using the k-points optimization procedure the number of k-points and the total energy is calculated. For the next step, the crystal is divided to 4 picese along x, y and z directions, which is 4x4x4 Monkhorst-Pack grid. For this and the next steps such as 6x6x6, 8x8x8 etc… the number of k-points and total energies are calculated by the k-point optimization procedure. The 2x2x2 grid is very rough calxulation, by increasing the number of grids the procedure becomes more precise and the number of k-poins increases. At the next step of this calculation, the total energy versus Monkhorst-Pack Grids and total energy versus number of k-points graphs can be plotted. In our study, Figure 4.3 (Figure 4.5) gives the total energy versus Monkhorst –Pack grid under GGA (under LDA) and, Figure 4.4 (Figure 4.6) gives the total energy versus number of k-points graph under GGA (under LDA). From those figures, it is noticed that arouns 8x8x8 grid the total energy becomes stable, but we decided the value of grid as 14x14x14 and accordingly the nember of k-points as 84 for the next calculations.

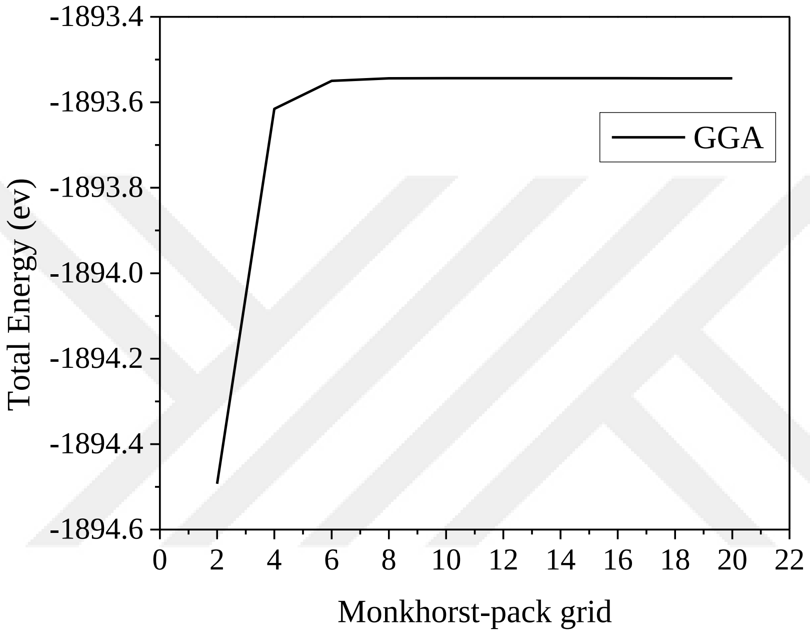

Figure 4.3. Total energy vs. Monkhorst-Pack Grid graph of $BaIrO_3$ crystal under GGA.

It is also noticed that the stable total energy values calculated from k-points optimization are -69.59 Ha for GGA and -69.71Ha for LDA which are very close to the values obtained from the cut-off energy calculations.

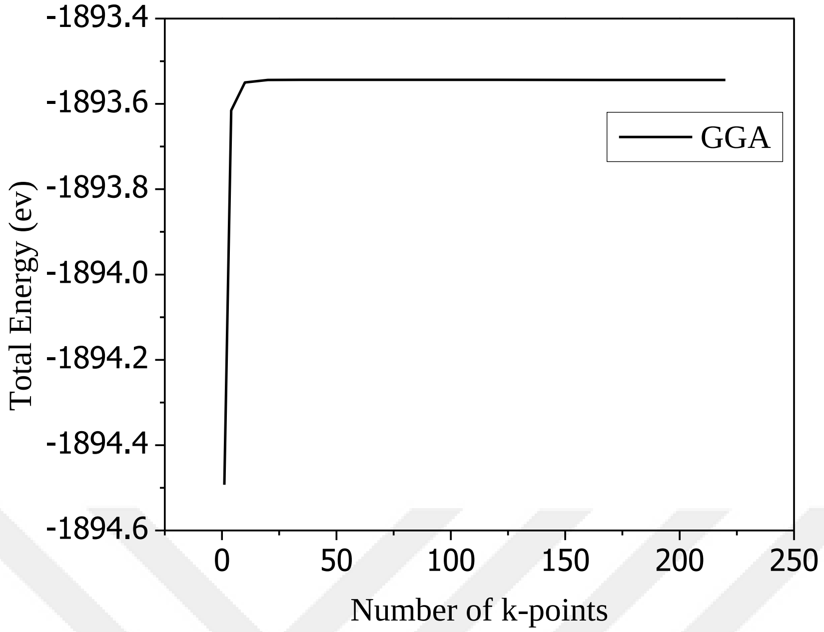

Figure 4.4. Total energy vs. number of k-points graph of $BaIrO_3$ crystal under GGA.

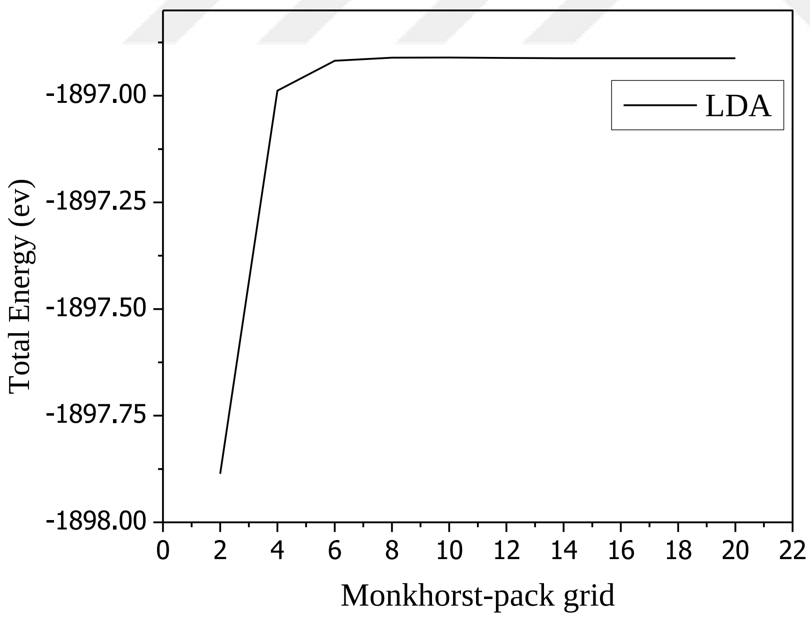

Figure 4.5. Total energy vs. Monkhorst-Pack Grid graph of $BaIrO_3$ crystal under LDA.

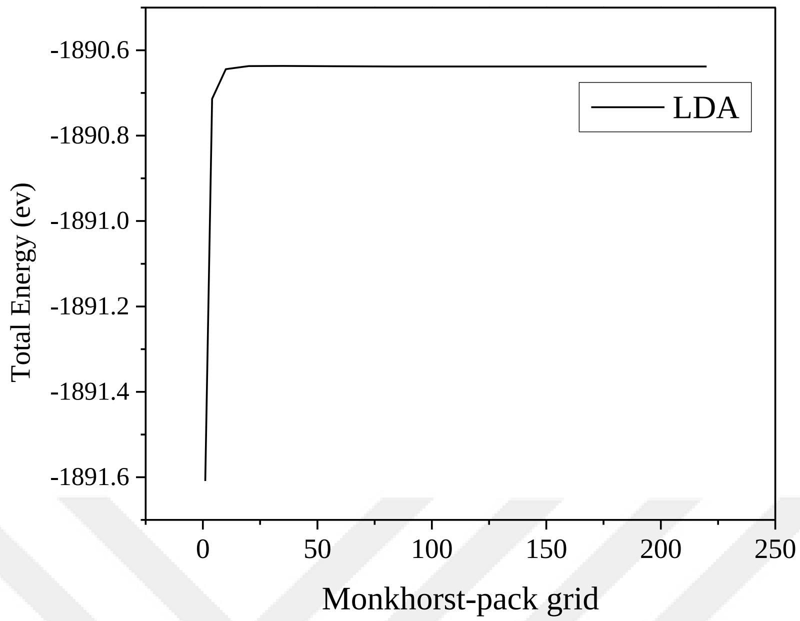

Figure 4.6. Total energy vs. number of k-points graph of $BaIrO_3$ crystal under LDA.

4.2.3. Volume optimization

In the volume optimization, we calculated the theoretical lattice parameters of $BaIrO_3$ crystal, its volume and total energy for the ground state of $BaIrO_3$, that is, the decisive state of the crystal. First, we plotted the total energy vs volume graph under GGA (Figure 4.7) and under LDA (Figure 4.8). From these graphs it is seen that the minimum point of the graph gives the stable state of the crystal. At that point the total energy value is -69.59 Ha for GGA and is -69.71 Ha for LDA, which are very close the previous results of this study. The volume of the $BaIrO_3$ for its stable state is calculated as 481.69 $Bohr^3$ under GGA and 451.38 $Bohr^3$ under LDA (Table 4.1). The lattice parameters of $BaIrO_3$ is calculated as 7.8389 Bohr for GGA and 7.6709 Bohr for LDA. The value of the lattice parameter in the literature is 7.7049 Bohr. So our theoretical values especially the value obtained under LDA is very close to the literature.

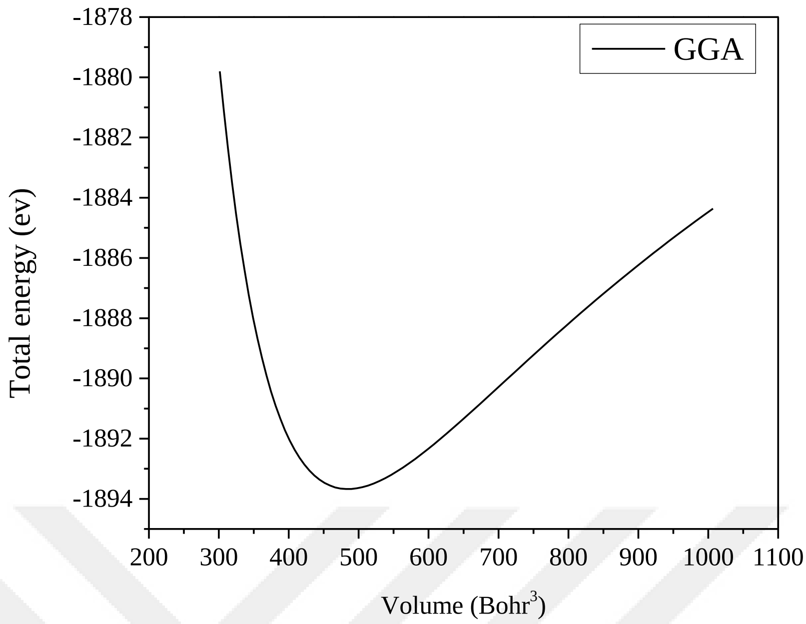

Figure 4.7. Total energy vs. volume graph of $BaIrO_3$ crystal under GGA.

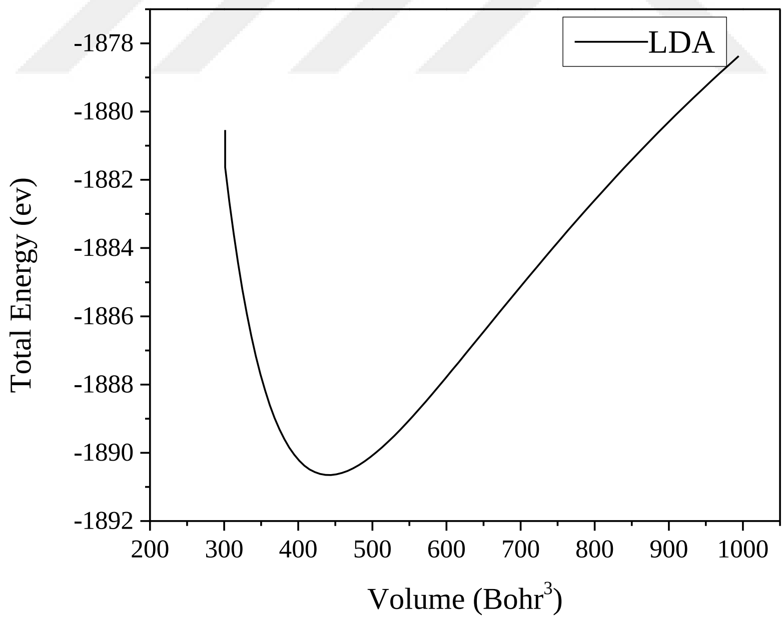

Figure 4.8. Total energy vs. volume graph of $BaIrO_3$ crystal under LDA.

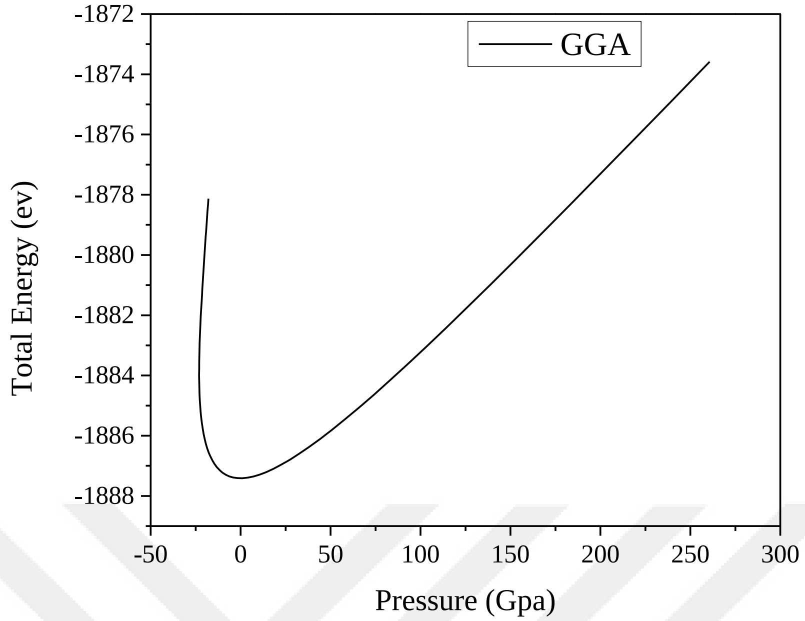

Figure 4.9. Total energy vs. pressure graph of $BaIrO_3$ crystal under GGA.

The total energy vs pressure graphs are given in Figure 4.9 for GGA and in Figure 4.10 for LDA. The minimum value of those graphs (0 GPa) corresponds to the stable state of the crystal, in other words the ground state og the crystal.

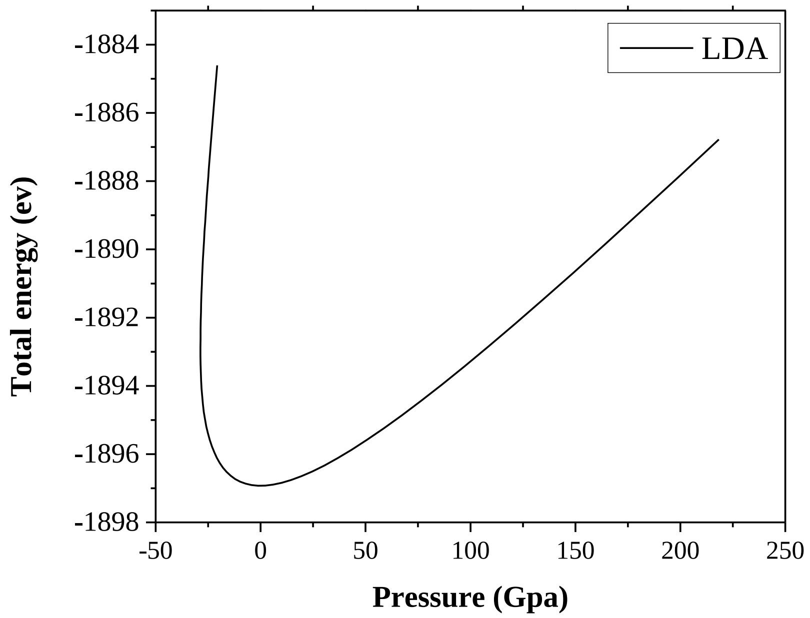

Figure 4.10. Total energy vs. pressure graph of $BaIrO_3$ crystal under LDA.

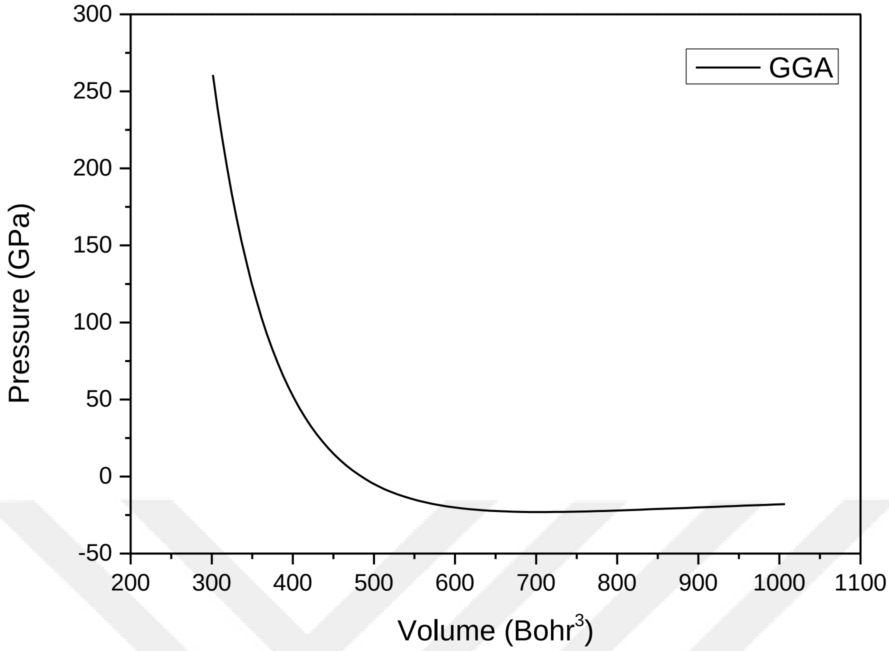

Figure 4.11. Pressure vs. volume graph of $BaIrO_3$ crystal under GGA.

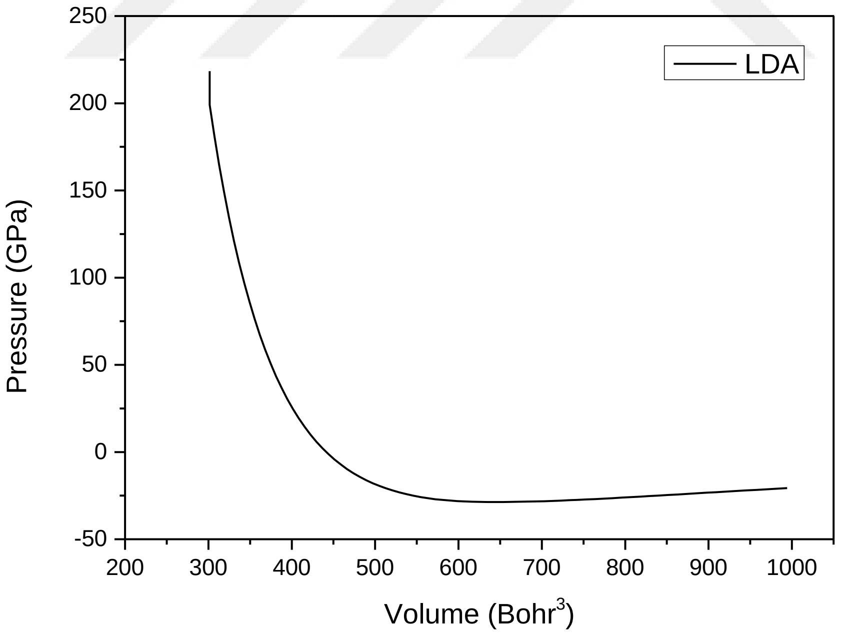

Figure 4.12. Pressure vs. volume graph of $BaIrO_3$ crystal under LDA.

The pressure versus volume graphs are given in Fig. 4.11 for GGA and in Fig. 4.12 for LDA. The behaviour of pressure with respect to the volume is inversely proportional as expected.

4.2.4. Lattice parameters of $BaIrO_3$ crystal

In the volume optimization we also calculated the lattice parameters (Table 4.1). As seen from Table 4.1, the lattice parameter value obtained under LDA is more close to the value obtained from the literature (Jain et al., 2013). We also plotted the total energy versus lattice parameter graph under GGA (Fig. 4.13) and LDA (Fig. 4.14). Since there were no data related with the total energy, we could not compare this with the literature.

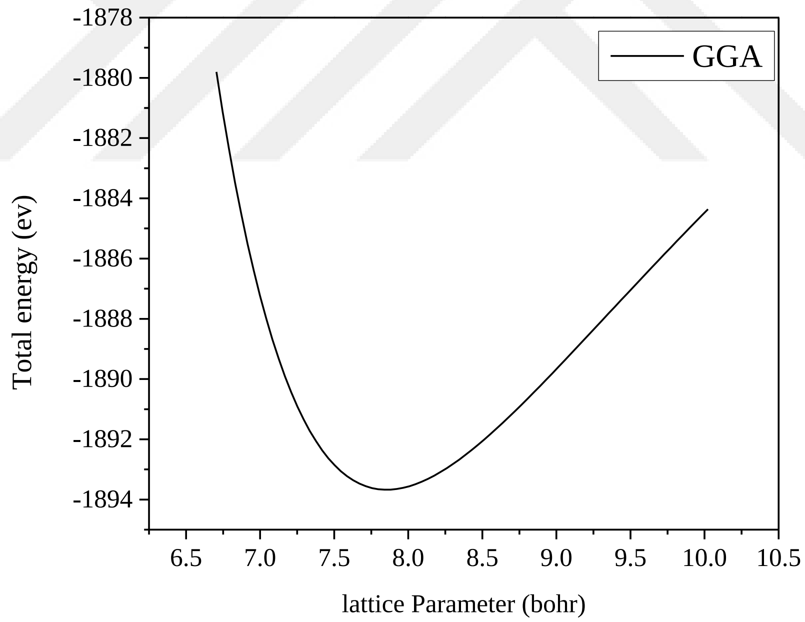

Figure 4.13. Total energy vs. lattice parameter graph of $BaIrO_3$ crystal under GGA.

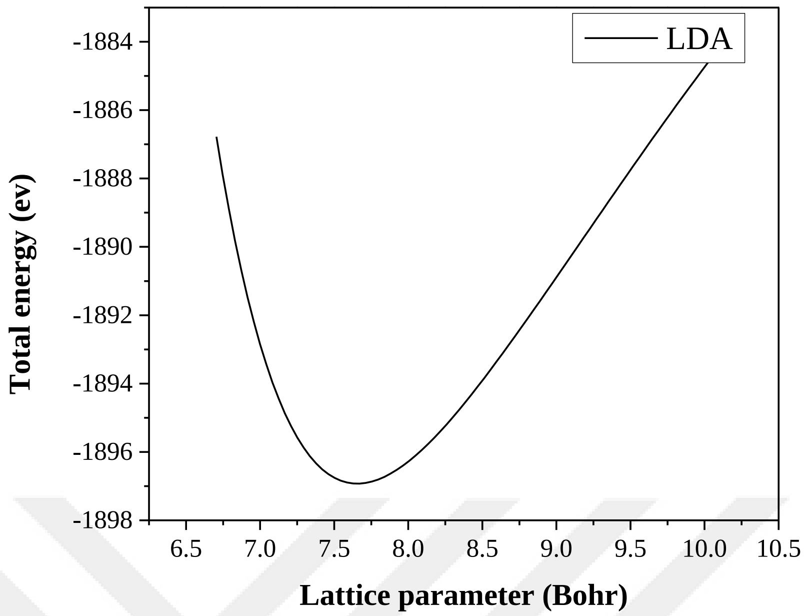

Figure 4.5. Total energy vs. lattice parameter graph of $BaIrO_3$ crystal under LDA.

Table 4.1. The calculated lattice parameter, volume and total energy values of $BaIrO_3$ crystal

	GGA	LDA	Literature (Jain et al., 2013)
Lattice Parameter (Bohr)	7.8389	7.6709	7.7049
Volume ($Bohr^3$)	481.69	451.38	457.40
Total Energy (eV)	-1893.6402	-1896.9056	---

As seen from the above table (4.1) also the volume value obtained under LDA approximation is closer to the value obtained from the literature.

4.2.5. Unit cell and bond lenghts of $BaIrO_3$ crystal

Here we obtained the unit cell structure of $BaIrO_3$ crystal, the bonds and the bond lenghts by Vesta computer programme. $BaIrO_3$ is a cubic crystal and it belongs to a perovskite structure. The space group of this crystal is $Pm\bar{3}m$ (No:221) and its point group is $m\bar{3}m$. We obtained the coordinates of the atoms in the unit cell of this crystal and we have shown it in Fig. 4.15. The bonds are between the Barium and Oxygen atoms and also between the Iridium and Oxygen atoms. We also calculate the lengths of these bonds and gave in Table 4.2.

Table 4.2. Bonds and the bond lengths in $BaIrO_3$ crystal

Bond	Bond Length (Bohr)
Ba-O	5.4482
Ir-O	3.8525

We also calculated the atomic coordinates and the Wcykoff positions of the atoms in the $BaIrO_3$, as can be seen from Table 4.3.

Table 4.3. The atomic coordinates and the Wcykoff positions of the atoms in the $BaIrO_3$ crystal

Atoms	Wcykoff Positions	x	y	z
Ba	1a	0.50	0.50	0.50
Ir	1a	0.00	0.00	0.00
O(1)	1a	0.00	0.00	0.50
O(2)	1a	0.50	0.00	0.00
O(3)	1a	0.00	0.50	0.00

The ABINIT and the Vesta can use the same type of input files. In other words, the results obtained from ABINIT and the Vesta are consentient to each other. In Figure 4.15, we have shown the unit cell of the $BaIrO_3$ with two different point of view in order to Show the structure clearly. The bonds are occured between the Barium–Oxygen atoms and the Iridium-Oxygen atoms as seen in Figure 4.15. There is no bond between the Barium and the Iridium atoms directly. The preovskite structure is also seen from this figure clearly.

The size of the atoms are plotted proportionally to their original atomic sizes. So the Barium atom is the biggest one and the Oxygen atoms are very small compared those.

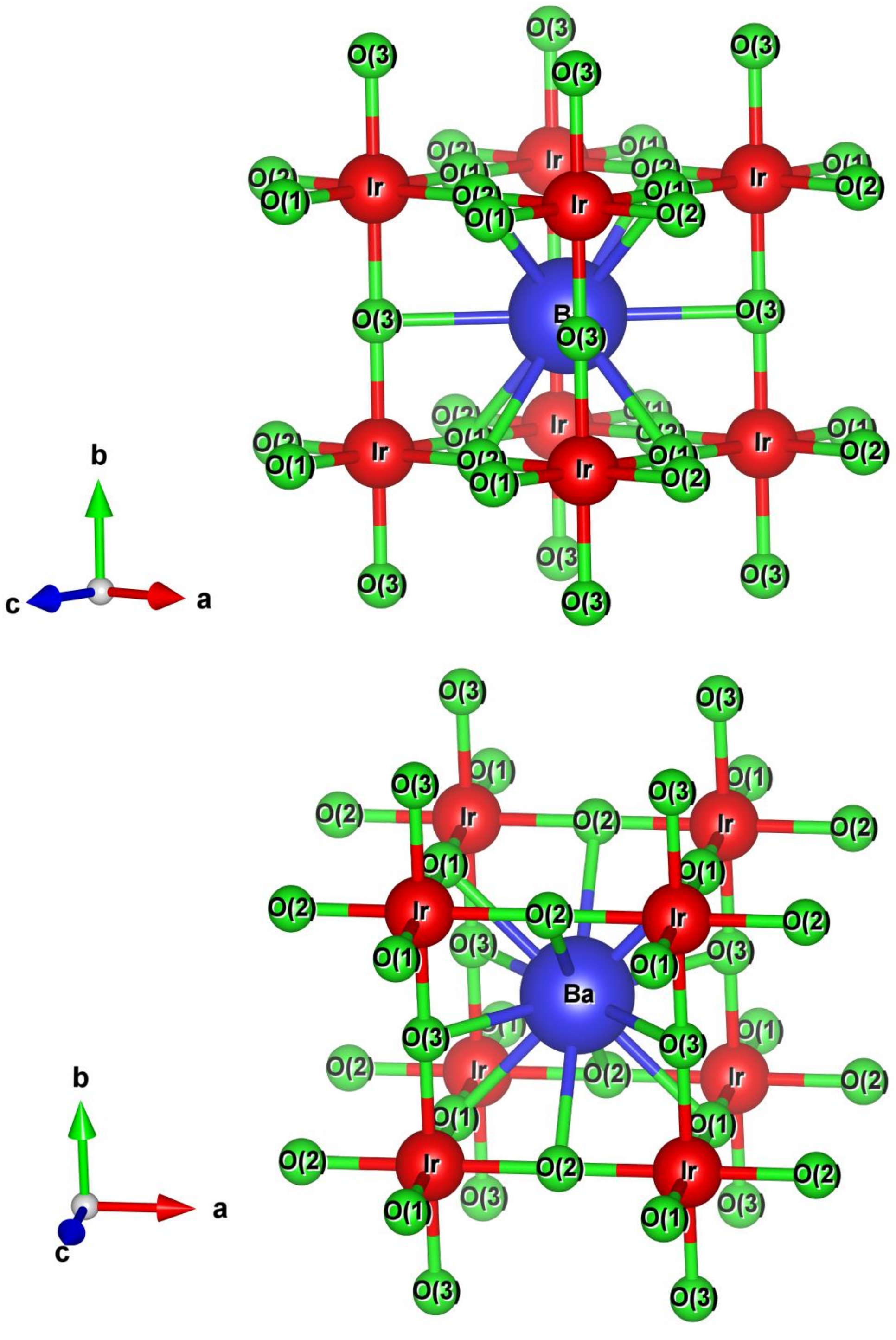

Figure 4.6. The unit cell of the $BaIrO_3$ crystal obtained by Vesta with two different point of views (Momma and Izumi, 2011).

4.3. The Electronic Properties of $BaIrO_3$ Crystal

In this stage of our thesis study, we investigated the electronic properties of $BaIrO_3$ crystal. In order to understand the electronic properties of $BaIrO_3$ cubic crystal, we calculated and plotted the electronic band structure, electronic density of states (DOS) and partial density of states graphs of the crystal. Electronic band structure graphes are calculated according to $\Gamma - X - M - \Gamma - R - X$ high symmetry points in the 1. Brillouin zone. The Cartesian coordinates of these high symmetry points are given in Table 4.4.

Table 4.4. The cartesian coordinates of the Γ-X-M-R high symmetry points in the first Brillouin zone

High Symmetry Points	Cartesian Coordinates in the First Brillouin Zone
Γ	$\frac{2\pi}{a}(0, 0, 0)$
X	$\frac{2\pi}{a}(0, \frac{1}{2}, 0)$
M	$\frac{2\pi}{a}(\frac{1}{2}, \frac{1}{2}, 0)$
R	$\frac{2\pi}{a}(\frac{1}{2}, \frac{1}{2}, \frac{1}{2})$

4.3.1. Electronic band structure

The electronic band structure of $BaIrO_3$ crystal calculated in both approximations namely, GGA and LDA. The electronic band structure graph for GGA (LDA) is given in Figure 4.16 (Figure 4.17). The energy states are given in eV units and the high energy points are $\Gamma - X - M - \Gamma - R - X$, respectively. Both of the figures are very similar to each other. We noticed that, there is a core electron energy levels around -20 eV energy values. The energy value of the top filled level (with the electrons) in the ground state is called as Fermi energy (E_F). Here we matched the Fermi energy level to 0 eV. In both figures the horizontal red line refers to Fermi energy level.

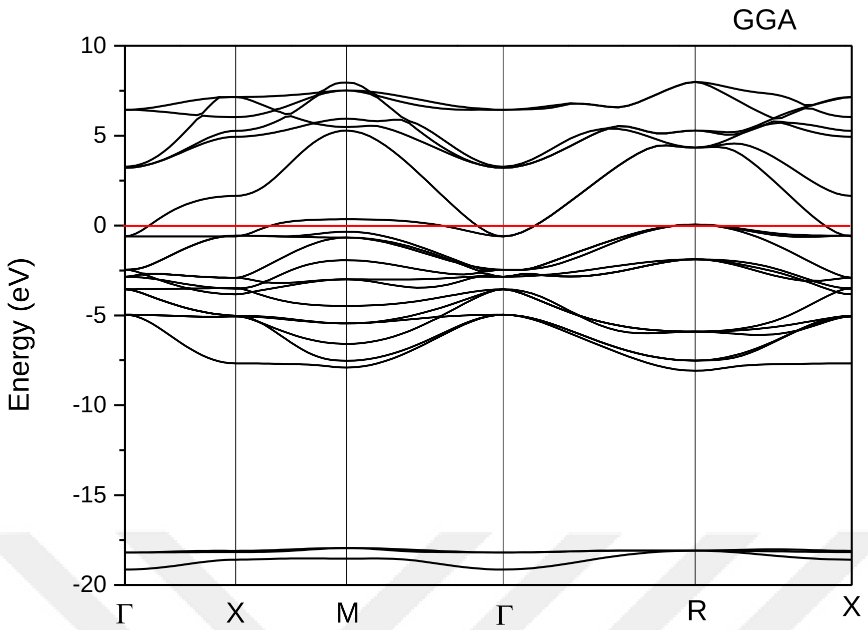

Figure 4.7. Electronic band structure of $BaIrO_3$ under GGA. The Fermi energy level is given with red horizontal line.

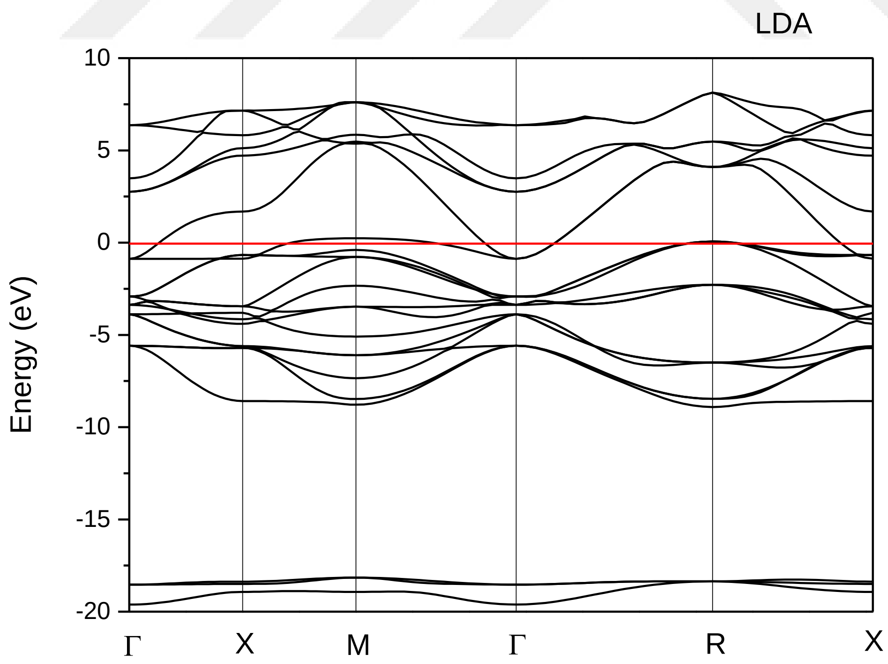

Figure 4.8. Electronic band structure of $BaIrO_3$ under LDA. The Fermi energy level is given with red horizontal line.

The electronic bands which have smallest energies than the Fermi energy level are known as valance bands and the ones with high energy levels than the Fermi level are known as conduction bands. $BaIrO_3$ crystal has 15 valance bands and the last one there is only one electron. We have shown 7 conduction bands in our graphs. Also it is noticed that there is no band gap in the electronic band structure graphs, so $BaIrO_3$ is a metal and it is a conductor.

4.3.2. Density of states (DOS)

After obtaining the electronic band structure we calculated the density of states (DOS) of $BaIrO_3$ under GGA (Figure 4.18) and LDA (Figure 4.19) approximations. The density of states are given in arbitrary units (a.u.) and the energy values are given in eV. The vertical red line refers to the Fermi energy level in both Figs. 4.18 and 4.19. It is seen that both of the density of states graphes obtained by two different approximations give nearly the same. The density of states graphs are also coincide with the electronic band structure graphs.

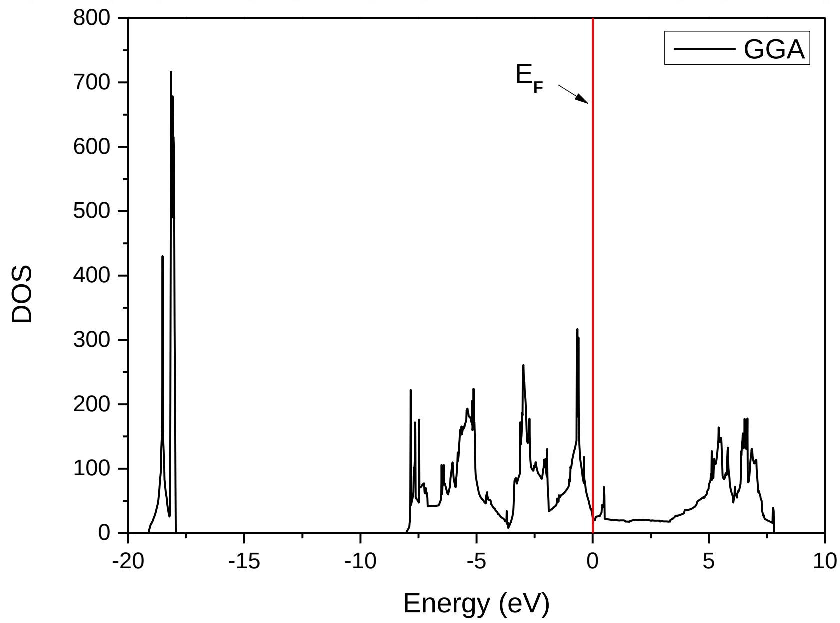

Figure 4.9. Density of states graph of $BaIrO_3$ crystal under GGA. The vertical red line shows the Fermi energy level.

The lower energy values than the Fermi level give the contribution of the valance bands and the higher energy values than the Fermi level show the contribution of the conduction bands to the density of states. Around -20 eV energy values the contribution of the core electrons can be seen. Also around Fermi level there is no band gap which shows that the $BaIrO_3$ crystal is a metal and it is a conductor.

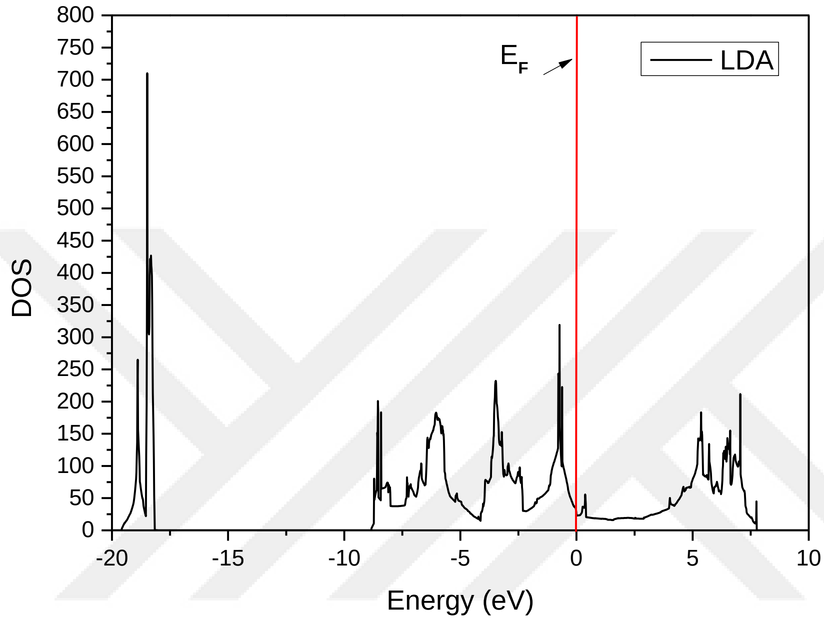

Figure 4.10. Density of states graph of $BaIrO_3$ crystal under LDA. The vertical red line shows the Fermi energy level.

4.3.3. Partial density of states (PDOS)

The density of states of an atom of each elements in a crystal is known as partial density of states (PDOS). Here we calculated the partial density of states of the Ba, Ir, and O atoms in both GGA and LDA approximations. Again the PDOS values are given in arbitrary units and the energy in eV. In the next 5 figures the PDOS graphs of Ba, Ir O(1), O(2) and O(3) atoms are given in the Figs. 4.20-4.24, respectively. After next 5 graphs are belong to the results of LDA approximation. We noticed that in both approximations the results are very close to each other.

In the partial density of states graphs the contributions of the s, p d and f states are also clearly given. Here “l” is the quantum number. l=0, 1, 2 and 4 refers to the s, p, d and f states, respectively.

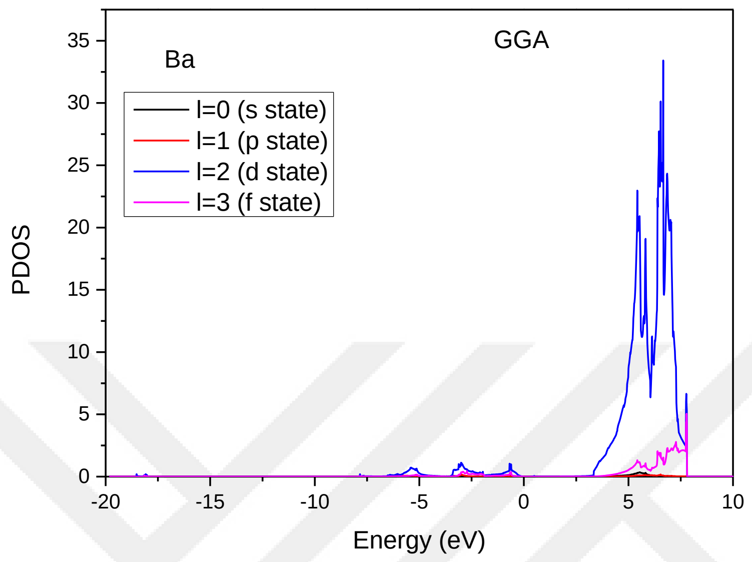

Figure 4.11. The partial density of states (PDOS) graph of Ba atom under GGA.

In Figs. 4.20 (GGA) and 4.25 (LDA) the PDOS graphs are of Ba atoms are given. It is seen that the main contribution of the Ba atoms come from the conduction bands and especially from the d state. However, there is a slight contribution which comes from the valance bands.

The contribution of Ir atoms to the density of states are seen from Figs. 4.21 (GGA) and 4.26 (LDA). The contribution of Ir atoms come from both valance and the conduction bands with mainly the d state. Also some contribution of core electrons come from Ir atoms as seen from these figures around -20 eV energy values.

It can be seen in Figs. 4.22 and 4.27 that the contribution of O(1) atoms are mostly from the valance bands. The contribution of core electrons are also quite high. The contribution of core electrons are composed of s state and the contribution of the valance bands are composed from p state. Also there is a slight contribution from the conduction band with p state.

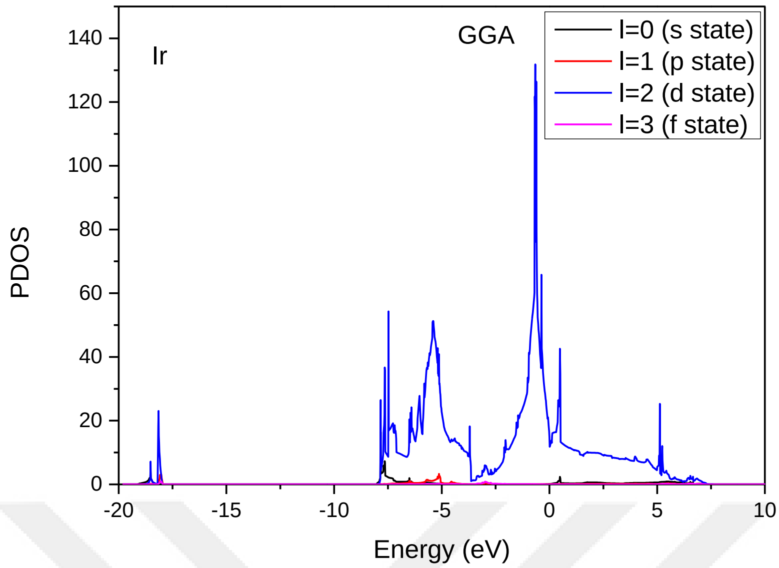

Figure 4.21. The partial density of states (PDOS) graph of Ir atom under GGA.

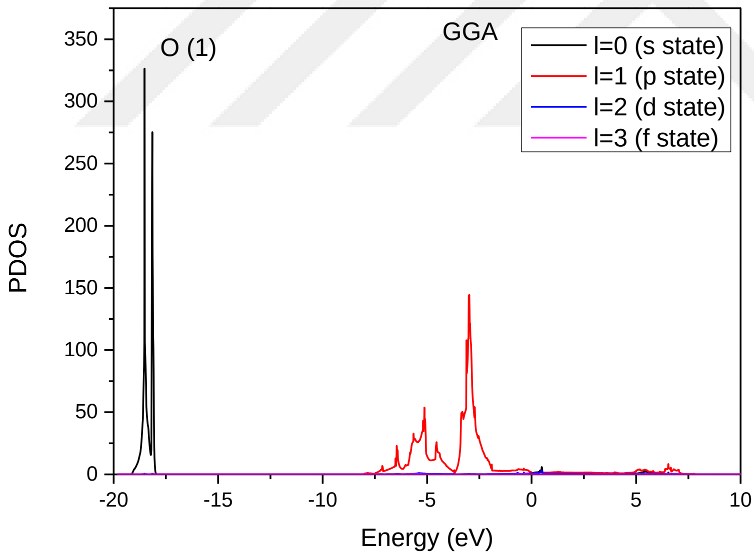

Figure 4.22. The partial density of states (PDOS) graph of O(1) atom under GGA.

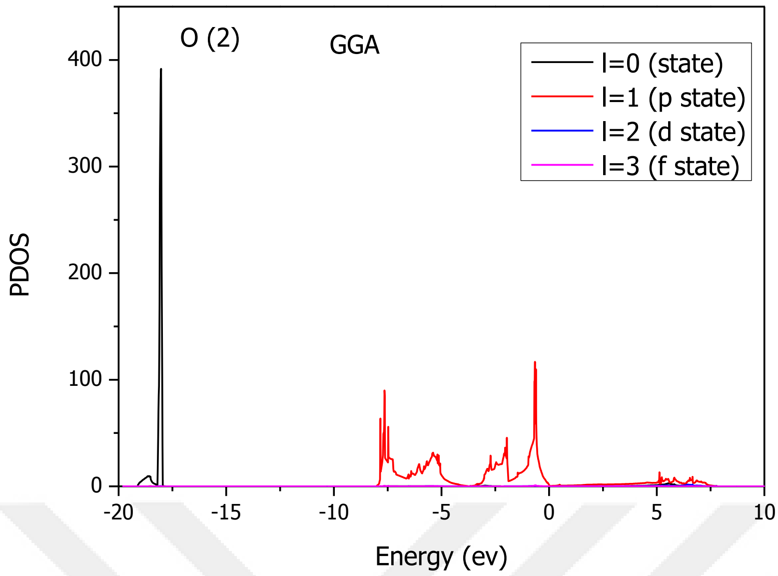

Figure 4.23. The partial density of states (PDOS) graph of O(2) atom under GGA.

The contribution of O(2) and O(3) atoms to density of states are similar to the O(1) atoms under both of the approximations (see Figs. 4.23, 4.28, 4.24 and 4.29). The main contribution comes from the valance bands within the core electron states. The contribution of the core electron levels composed mainly from s states. The contribution of rest of the valance bands are coposed mainly of p states. As a summary the contribution of conduction bands are mainly come from Ba and Ir atoms, and of valance bands are from the O(1), O(2) and O(3) atoms.

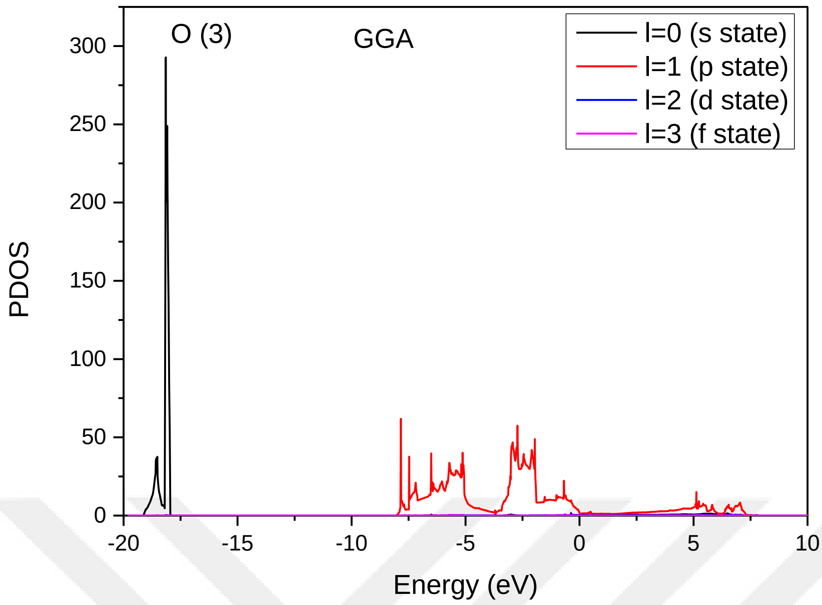

Figure 4.24. The partial density of states (PDOS) graph of O(3) atom under GGA.

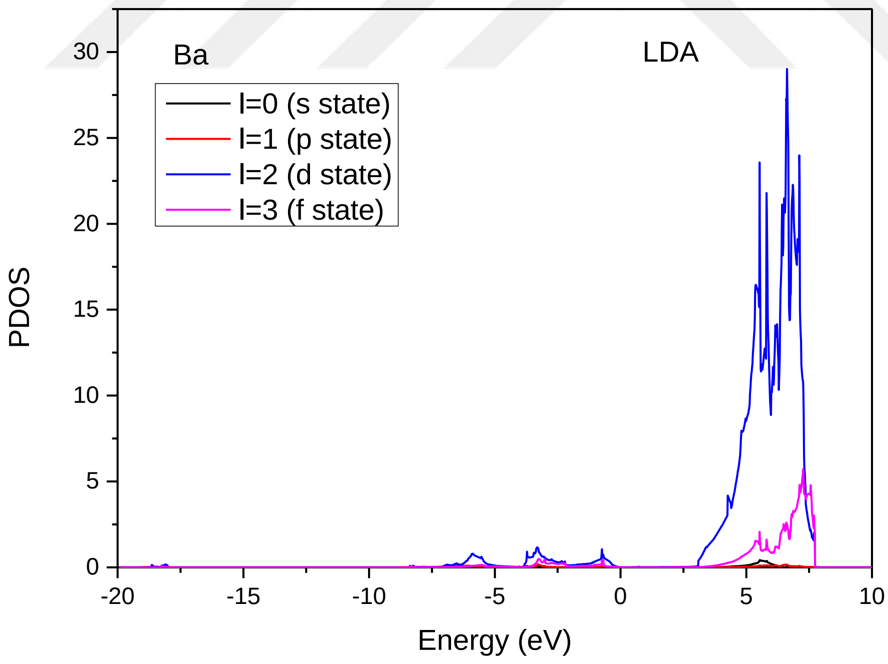

Figure 4.25. The partial density of states (PDOS) graph of Ba atom under LDA.

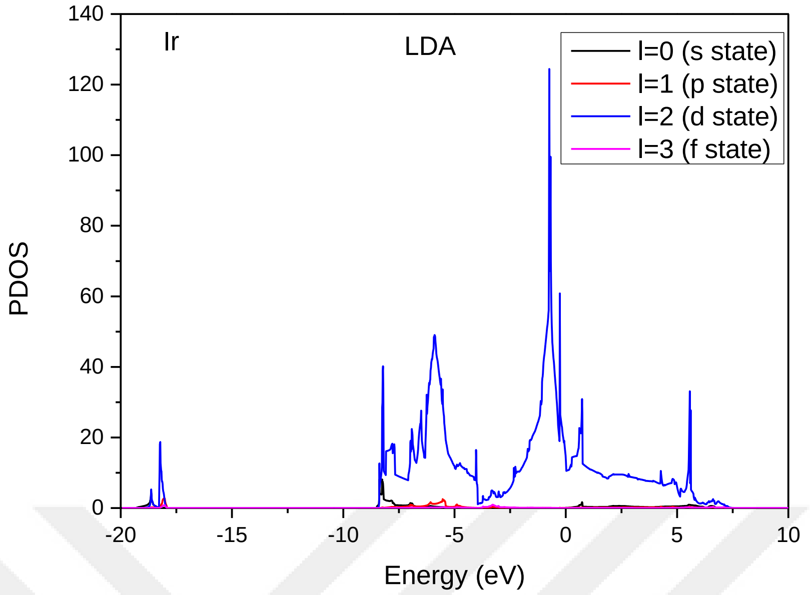

Figure 4.26. The partial density of states (PDOS) graph of Ir atom under LDA.

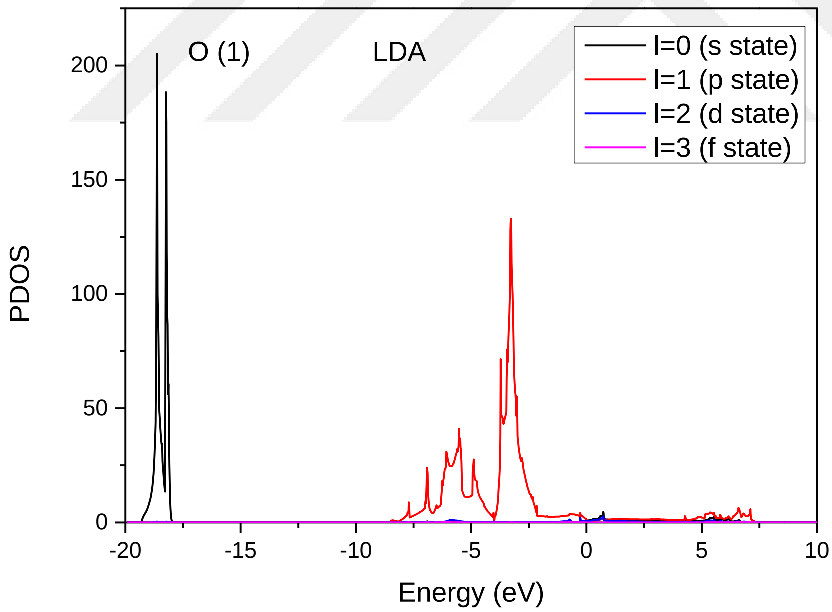

Figure 4.27. The partial density of states (PDOS) graph of O(1) atom under LDA.

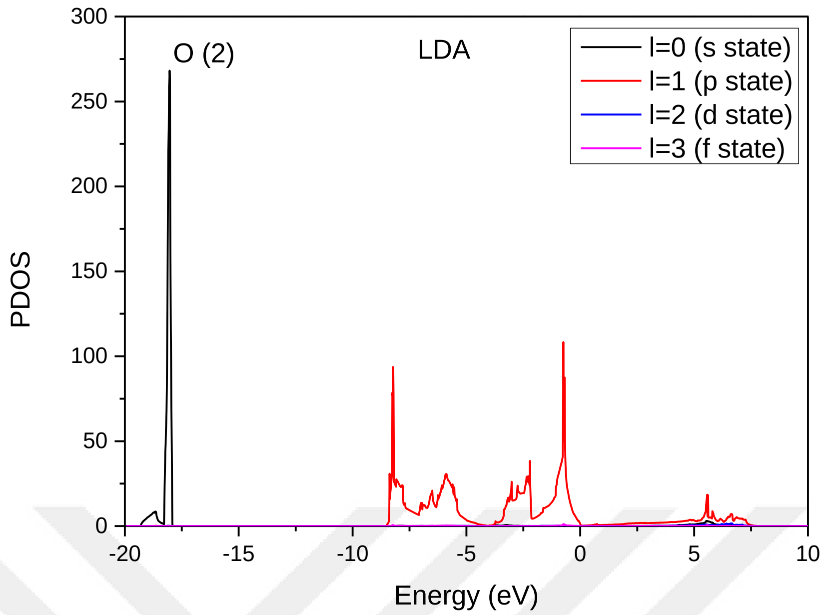

Figure 4.28. The partial density of states (PDOS) graph of O(2) atom under LDA.

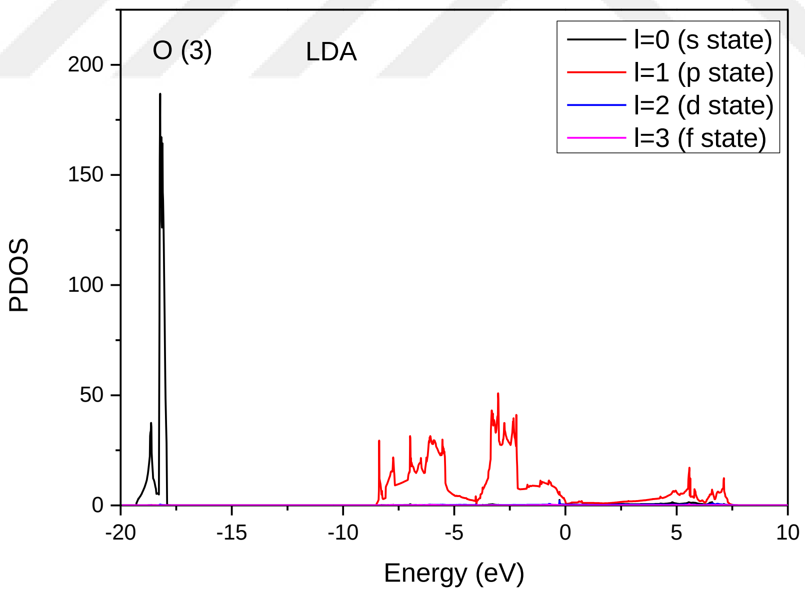

Figure 4.29. The partial density of states (PDOS) graph of O(3) atom under LDA.

The addition of those partial density of states (PDOS) under the same approximation gives the total density of states (DOS). So it is clearly seen that the addition of e.g. Figs. 4.20-4.24 (Figs. 4.25-4.29) gives Fig. 4.18 (Fig. 4.19).

4.4. The Elastic Properties of $BaIrO_3$ Crystal

In order to investigate the elastic properties of $BaIrO_3$ cubic crystal, we calculated the elastic stiffness constants (C_{ij}) and the elastic compliance constants (S_{ij}) and gave in Table 4.5 and 4.6, respectively. Again, as the previous calculations, we performed all elastic computations under two approximations, namely, GGA and LDA. Here our results again close to each other but not as much as the structural propery and electronic property calculations. Since the calculated lattice parameter value of LDA approximation is more close to the literature value. So we can accept the results of LDA also for the elastic calculations.

Table 4.5. The calculated elastic stiffness constants of $BaIrO_3$ crystal under GGA and LDA approximations

Elastic Stiffness Constants	GGA (GPa)	LDA (GPa)
C_{11}	247.65	298.82
C_{12}	115.59	130.90
C_{44}	71.02	79.91

Table 4.6. The calculated elastic compliance constants of $BaIrO_3$ crystal under GGA and LDA approximations

Elastic Compliance Constants	GGA $(GPa)^{-1}$	LDA $(GPa)^{-1}$
S_{11}	0.0040	0.0033
S_{12}	0.0086	0.0076
S_{44}	0.0140	0.0125

The elastic stiffness and the elastic compliance constants are inversely proportional, in other words the multiplication of these two constants equal to 1 ($C_{ij} = \frac{1}{S_{ij}}$). This fact can be checked from the Table 4.5 and 4.6. The units of elastic stiffnes constant is GPA and the unit of elasric compliance constant is GPa^{-1}.

We checked the mechanical stability of our crystal $BaIrO_3$ by using the Born stability criteria (Mouhat and ark, 2014). If the elastic stiffness constants of a material obeys those criteri, then it can be said that material is mechanically stable. Those Born criteria are given in the following equation.

$$C_{11} + 2C_{12} > 0,\ C_{44} > 0,\ C_{11} - C_{12} > 0\ ,\quad C_{11} > 0 \text{ and } C_{12} < B < C_{11} \tag{4.3}$$

where B is the Bulk modulus. It is noticed that since the elastic stiffness constants obeys those criteri, $BaIrO_3$ is mechanically stable.

In the previous chapter, we mention about Bulk modulus. Here we also calculated the Bulk and Shear modulus with three different approaches, namely, Voight, Reuss ve Hill. The calculated values of Bulk modulus with respect to three approaches have the same result. Also, those results of Shear modulus are very close to each other. We also calculated the Young modulus, Poisson ratio, flexibility coefficient and Zener anisotropy factor under GGA and LDA (Table 4.7).

The force per unit area is called stress. If a force applied on a material, it generally causes a deformation on the shape of that material. This deformation is called strain. This deformation can be temporary or permanent which belongs to both the strenght of the force and the elastical feature of the material. If the shape of a body returns to it is original state by removing the force then these kind of bodies called elastic materials. But if the deformation lasts, the body can not return to its original shape after removing the force, then these bodies are called non-elastic (or fragile) bodies. In this study we also examined the elastic feauture of the $BaIrO_3$ crystal. There are some ways to check this feature. First we used Cauchy pressure test that is, if the value of $C_{12} - C_{44}$ expression is positive then the material is elastic, but if it is negative the material is fragile. Table 4.5 shows that C_{12} is bigger than C_{44}, so Caucht pressure expression is positive for $BaIrO_3$, which shows $BaIrO_3$ is an elastic material. Also we can check by calculating the flexibility constant (K). The critical value for this constant is 1.75. If the calculated flexibility constant is bigger that that value the material is elastic. But if the calculated value of the flexibility constant is smaller that 1.75 then this material is fragile material. Since our calculated flexibility constant value is bigger than 1.75 under both of the approximations. So our material is elastic material. The last test on this issue is the poisson ratio. If the calculated value of the poisson ratio is bigger that 0.3 then this material is elastic, if not then this material is fragile. Our calculated value of poisson ratio is bigger than 0.3 under GGA and LDA, so we proved that $BaIrO_3$ is an elastic material (Table 4.7).

Table 4.7. Some elastic modulus and constants of $BaIrO_3$ crystal under GGA ve LDA approximations

The Elastic Properties	Symbol (Unit)	GGA	LDA
Voight Bulk Modulus	B_V (GPa)	159.61	186.88
Reuss Bulk Modulus	B_R (GPa)	159.61	186.88
Hill Bulk Modulus	B_H (GPa)	159.61	186.88
Voight Shear Modulus	G_V (GPa)	69.03	81.54
Reuss Shear Modulus	G_R (GPa)	68.94	81.49
Hill Shear Modulus	G_H (GPa)	68.98	81.51
Young Modulus	E (GPa)	180.89	213.49
Poisson Ratio	v (-)	0.311	0.310
Flexibility Constant	$K=B_{VRH}/G_{VRH}$ (-)	2.314	2.293
Zener Anizotropy Factor	A (-)	1.00	0.95

In this study we also studied on the Zener anisotropy factor. Isotropy means uniformity in all directions. An isotropy has the opposite meaning. If a material is anisotropic behaviour on a physical property, that means, that physical property changes according to different directions or orientations. Here Zener anisotropy factor gives the information if the elastic properties of that material isotropic or not. If the calculated value of Zener anisotropy factos is 1 or very close to 1, then that material has isotropic property. But if that value is far avay 1, then that material is anisotropic material. Our calculated value of Zener anisotropy factor is 1 for GGA and 0.95 for LDA so $BaIrO_3$ is an isotropic material .

5. CONCLUSION

In this study we examined the structural, electronic and elastic properties of $BaIrO_3$ cubic crystal by Density Functional Theory within Generalized Gradient Approximation and Local Density Approximation using ABINIT computer programe.

We start our study by calculating the cut-off energy and the number of k-point values by performing cut-off energy and k-point optimisations, respectively. Once we found those values we used them throughout all our calculation in this thesis study. We calculated the theoretical lattice parameter. Our theoretical lattice parameter values with respect to both approximations are very close to the value that we found from the literature, but one within the LDA approximation is more close to the literature value. In the structural property investigation we also calculated the total energy, volume of $BaIrO_3$ in its stable state. We also plotted the pressure versus volume behaviour of $BaIrO_3$ crystal. In this frame we obtained the unit cell scheme, bonds and bond lengths of $BaIrO_3$ by using Vesta computer programme.

After the structural properties we investigated the electronic properties of $BaIrO_3$ cubic crystal. In this stage we computed and plotted the electronic band structure, density of states, and the partial density of states of our crystal under GGA and LDA. For those calculations Fermi energy level is matched to 0 eV energy value, in order to be able to compare the bands clearl. We saw that all results are consistent to each other. From those graphs, it is noticed that $BaIrO_3$ is a metal structure and it is a conductor. From electronic band structure graphs the core electron, valance and the conduction bands can be seen clearly. Also density of states graphs show the contributions of core, valance and conduction bands. By looking to the partial density of states graphs, one can see the all contributions of all s, p, d and f electronic states of all type of atoms in $BaIrO_3$ crystal.

After all, we examined the elastic properties of $BaIrO_3$ cubic crystal. We calculated elestic stiffnes constants and elastic compliance constants. After wards, by using those constants we investigated the mechanically stability of $BaIrO_3$ by using Born stability criterias. It is shown that our crystal is mechanically stable. Also we calculated the Bulk, Shear and Young modulus, Poisson ratio, Flexibility constant and

Zener anisotropy factor under LDA and GGA approximations. After elastic computation we noticed that $BaIrO_3$ is an elastic and elastically isotropic material.

All the results of those calculations of this study is given by graphs and tables throughout the thesis. Except for the lattice constant calculation, the all the results are obtained for the first time with this thesis study. We believe that this thesis will be a reliable source on $BaIrO_3$ crystal and it will shed light on new studies and the researchers.

In future study the optical properties of $BaIrO_3$ theoretically can be investigated and deternine many optical constant. After performing the study could be decide on whether this crystal is suitable for optical applications or not. Furthermore thermodynamic and dynamical properties of $BaIrO_3$ can be study. Using this properties also many thermodynamic constants can be explored. Additionally stucture, electronic and elastic properties of $BaIrO_3$ repeated via differrent program such as WIN2K software.

REFERENCES

Alexander, S., Orbach, R., 1982. Density of states on fractals:«fractons». ***Journal de Physique Lettres***, **43** (17): 625-631.

Amusia, M. Y., Msezane, A., Shaginyan, S., 2003. Density functional theory versus the hartree–fock method. ***Comparative assessment,*** **68** (6): C133.

Babilas, R., Mlynarek, K., Lonski, W., Lukowiec, D., Kadziolka-Gawel, M., Czeppe, T., Temleitner, L., 2020. Structural Characterization of Al65Cu20Fe15 Melt-Spun Alloy by X-ray, Neutron Diffraction, High-Resolution Electron Microscopy and Mossbauer Spectroscopy. ***Materials (Basel),*** **14** (1): 54-64.

Barr, A., Barr, A., Porter, D., Reichl, S., 2017. Signatures of chaos in the Brillouin zone. ***Chaos: An Interdisciplinary Journal of Nonlinear Science,*** **27** (10): 104604-104613.

Bauernschmitt, R., Ahlrichs, R., 1996. Stability analysis for solutions of the closed shell Kohn–Sham equation. ***The Journal of Chemical Chysics,*** **104** (22): 9047-9052.

Bornath, T., Kremp, D.,Schlanges, E., 1999. Two-particle problem in a nonequilibrium many-particle system. ***Physical Review E,*** **60** (6): 6382-6394.

Bown, M., Gay, M., 1959. The reciprocal lattice geometry of the plagioclase felspar structures. ***Zeitschrift für Kristallographie-Crystalline Materials,*** **111** (1-6): 1-14.

Burke, K., Perdew, P., Ernzerhof, C., 1997. Why the generalized gradient approximation works and how to go beyond it. ***International Journal of Quantum Chemistry,*** **61** (2): 287-293.

C.Kittel. ***Intoroduction to Solid State Physics*** egiht ed.: John Wiley & Sons, Ins.

Castro, A., Marques, M., Rubio, A., 2004. Propagators for the time-dependent Kohn–Sham equations. ***The Journal of Chemical Physics,*** **121 (**8): 3425-3433.

Chen, Q., De Marco, N., Yang, M., Song, B., Chen, C., Zhao, H., Yang, T., 2015. Under the spotlight: The organic–inorganic hybrid halide perovskite for optoelectronic applications. ***Nano Today,*** **10** (3): 355-396.

Cheng, G., Alonso, A., Suard, E., Zhou, S., Goodenough, J., 2009. A new perovskite polytype in the high-pressure sequence of $BaIrO_3$. ***Journal of the American Chemical Society,*** **131** (21): 7461-7469.

Combes, M., Duclos, P.,Seiler, R., 1981. The born-oppenheimer approximation. In *Rigorous atomic and molecular physics* (pp. 185-213): Springer.

Cowan, R., Ashkin, R., 1957. Extension of the Thomas-Fermi-Dirac statistical theory of the atom to finite temperatures. **Physical Review, 105** (1): 144-150.

Della Sala, F., Gorling, P., 2001. Efficient localized Hartree–Fock methods as effective exact-exchange Kohn–Sham methods for molecules. ***The Journal of Chemical Physics,*** **115** (13): 5718-5732.

Ebalard, S., Spaepen, R., 1989. The body-centered-cubic-type icosahedral reciprocal lattice of the Al–Cu–Fe quasi-periodic crystal. ***Journal of Materials Research,*** **4** (1): 39-43.

Epstein, S., Rosenthal, P., 1976. The Hohenberg–Kohn theorem. ***The Journal of Chemical Physics,*** **64** (1): 247-249.

Gavezzotti, C., 2011. Computational studies of crystal structure and bonding. ***Advanced X-ray Crystallography,*** 1-32.

Geerlings, P., De Proft, F., Langenaeker, R., 2003. Conceptual density functional theory. ***Chemical reviews,*** **103** (5): 1793-1874.

Ghosh, D., 2005. Three- dimensional structures of sulfatases. ***Methods in enzymology,*** **400**: 273-293.

Gorelov, V., Ceperley, M., Holzmann, M., Pierleoni, P., 2020. Electronic structure and optical properties of quantum crystals from first principles calculations in the Born–Oppenheimer approximation. ***The Journal of Chemical Physics,*** **153** (23): 234-240.

Görling, A., &Levy, M., 1997. Hybrid schemes combining the Hartree–Fock method and density-functional theory: Underlying formalism and properties of correlation functionals. ***The Journal of Chemical Physics***, **106** (7): 2675-2680.

Heo, D. Y., Do, H., Ahn, H.,Kim, P., 2020. Metal-organic framework materials for perovskite solar cells. **Polymers, 12** (9):2061-2070.

Hill, M., Solids, P., 1963. Elastic properties of reinforced solids: some theoretical principles. ***Journal of the Mechanics and Physics of Solids,*** **11** (5): 357-372.

Humphreys, J., 2013. The significance of Bragg's law in electron diffraction and microscopy, and Bragg's second law. ***Acta Crystallogr A,*** **69** (1): 45-50. doi:10.1107/S0108767312047587

Humphreys, C., 2013. The significance of Bragg's law in electron diffraction and microscopy, and Bragg's second law. ***Acta Crystallographica Section A: Foundations of Crystallography,*** **69** (1): 45-50.

Jain, A., Ong, P., Hautier, G., Chen, W., Richards, D., Dacek, S.,Ceder, A., 2013. Commentary: The Materials Project: A materials genome approach to accelerating materials innovation. ***APL materials,*** **1** (1): 110-119.

Juan,M.,Kaxiras, E., Gordon, B., 1995. Use of the generalized gradient approximation in pseudopotential calculations of solids. ***Physical Review B,*** **51**(15): 9521.

Kacher, J., Landon, C., Adams, L., Fullwood, D., 2009. Bragg's Law diffraction simulations for electron backscatter diffraction analysis. ***Ultramicroscopy,*** **109** (9):1148-1156.

Khan, A., Vazquez, M., Fernandes, M., Spectroscopy, B., 2021. Assessment of the proposed pseudo-potential theoretical model for the static and dynamic Raman scattering intensities: Multivariate statistical approach to quantum-chemistry protocols. **Spectrochimica Acta Part A: Molecular and Biomolecular Spectroscopy, 245**: 118-129.

Laguna, A., Haskel, D., Souza, N., Lang, J., Krishnamurthy, V., Chikara, S., Veenendaal, M., 2010. Orbital magnetism and spin-orbit effects in the electronic structure of $BaIrO_3$. **Physical review letters, 105** (21): 216407.

Li, S., 2006. Classification of Solids and Crystal Structure. *Semiconductor Physical Electronics* (pp. 1-25): Springer.

Lovett, B., Crosnier, C., Perarnau, M., Sanders, B., 2013. Differential evolution for many-particle adaptive quantum metrology. **Physical review letters, 110** (22): 220501.

Momma, K., Izumi, F., 2011. VESTA 3 for three-dimensional visualization of crystal, volumetric and morphology data. ***Journal of Applied Crystallography,*** **44** (6): 1272-1276.

Park, B., Chung, J., Jung, J., Sohn, K., Singh, S., Pyo, M., Sohn, K., 2017. Classification of crystal structure using a convolutional neural network. ***IUCrJ,*** **4** (4): 486-494.

Payne, C., Teter, P., Allan, C., Arias, T., Joannopoulos, R., 1992. Iterative minimization techniques for ab initio total-energy calculations: molecular dynamics and conjugate gradients. ***Reviews of modern physics,*** **64** (4): 1045-1052.

Raj, A., Biju, S., Reddy, M., 2008. One-, two-, and three-dimensional arrays of Eu3+-4, 4, 5, 5, 5-pentafluoro-1-(naphthalen-2-yl) pentane-1, 3-dione complexes: synthesis, crystal structure and photophysical properties. ***Inorganic chemistry,*** **47** (18): 8091-8100.

Sahni, A., 1997. Physical interpretation of density-functional theory and of its representation of the Hartree-Fock and Hartree theories. ***Physical Review A,*** **55** (3): 184-191.

Seidl, A., Gorling, A., Vogl, P., Majewski, A., Levy,B., 1996. Generalized Kohn-Sham schemes and the band-gap problem. ***Physical Review,*** **53** (7): 57-64.

Slater, R., 1953. A generalized self-consistent field method. ***Physical Review,*** **91**(3), 528-533.

Stampfl, C., Van de Walle, B., 1999. Density-functional calculations for III-V nitrides using the local-density approximation and the generalized gradient approximation. ***Physical Review B,*** **59** (8): 552-563.

Stoumpos, C., Kanatzidis, M., 2016. Halide Perovskites: poor Man's high- performance semiconductors. ***Advanced Materials,*** **28** (28): 5778-5793.

Tancogne, N., Mucke,D., Kartner, X., Rubio, A., 2017. Impact of the electronic band structure in high-harmonic generation spectra of solids. ***Physical review letters,*** **118** (8): 832-844.

Thogersen, L., Olsen, J., Yeager, D., Jørgensen, P., Sałek, P., Helgaker, T., 2004. The trust-region self-consistent field method: Towards a black-box optimization in Hartree–Fock and Kohn–Sham theories. ***The Journal of chemical physics***, **121**(1): 16-27.

Yabana, K., Bertsch, G., 1996. Time-dependent local-density approximation in real time. ***Physical Review B,*** **54** (7): 4484-4489.

Zhang, W., Eperon, E., Snaith, H., 2016. Metal halide perovskites for energy applications. ***Nature Energy,*** **1** (6): 1-8.

Zhao, J., Yang, R., Jin, C., 2009. Structural and physical properties of the 6M $BaIrO_3$: a new metallic iridate synthesized under high pressure.***Inorganic chemistry,*** **48** (10): 4290-4294.

EXTENDED TURKISH SUMMARY
(GENİŞLETİLMİŞ TÜRKÇE ÖZET)

PEROVSKİT $BaIrO_3$ KRİSTALİNİN BAZI FİZİKSEL ÖZELLİKLERİNİN YOĞUNLUK FONKSİYONELİ TEORİSİ İLE İNCELENMESİ

RZGAR SOR, Hawzhin
Yüksek Lisans Tezi, Fizik Anabilim Dalı
Tez Danışmanı: Doç. Dr. Emel KİLİT DOĞAN
Eylül 2021, 69 sayfa

Bu tez çalışmasında, $BaIrO_3$ perovskit kristalinin birtakım fiziksel özellikleri Yoğunluk Fonksiyoneli Teorisi ile Genelleştirilmiş Gradyent Yaklaşımı ve Yerel Yoğunluk Yaklaşımları altında incelenmiştir. $BaIrO_3$ kristalinin yapısal, elektronik ve elastik özellikleri ABINIT, birim hücresinin çizdirilmesi, bağ yapılarının incelenmesi ve bağ uzunluklarının hesaplanması ise VESTA bilgisayar programıyla yapılmıştır.

İlk olarak, yapısal özelliklerin incelenebilmesi için hacim optimizasyonu ile örgü parametresi teorik olarak hesaplanmıştır. Hesaplanan örgü parametresi değerlerinden Yerel Yuğunluk Yaklaşımı altında elde edilen değerin literatürdeki değere daha yakın olduğu görülmüştür. Yine bu aşamada $BaIrO_3$ kristalinin birim hücresi çizdirilmiş ve bağ yapısı ve bağ uzunlukları incelenmiştir. Ardından elektronik band yapı, durum yoğunluğu ve kısmi durum yoğunluğu grafikleri çizdirilerek $BaIrO_3$ kübik kristalinin elektronik özellikleri ortaya konmuştur. Son olarak $BaIrO_3$ kristalinin elastik özelliklerini inceleyebilmek için elastik sertlik ve elastik uyum katsayıları hesaplanmıştır. Bu değerler kullanılarak temel elastik özellikler hesaplanmıştır. Buradan kristalin elastik olarak kararlı bir yapıda olup esnek yapıya sahip bir malzeme olduğu ortaya konmuştur. Elde edilen tüm sonuçlar grafik ve tablolarla kıyaslamalı olarak verilmiştir. Literatürde bu kristal ile ilgili benzer bir çalışmayla karşılaşılmadığından, bu çalışmanın $BaIrO_3$ kübik kristali ile yapılacak olan çalışmalara ışık tutacağı düşünülmektedir.

Anahtar kelimeler: ABINIT, $BaIrO_3$, Durum yoğunluğu, Elastik özellikler, Elektronik özellikler, Kısmı durum yoğunluğu, Yoğunluk fonksiyoneli teorisi

1. MATERYAL VE YÖNTEM

Malzemelerin fiziksel özelliklerinin anlaşılabilmesi için zamandan bağımsız Schrödinger denklemlerinin çözülmesi gerekir. Ancak malzemeler çok sayıda atom ve moleküllerden oluştuğundan ve onlarda çok sayıda elektron içerdiklerinden, malzeme içinde çok fazla etkileşme vardır. Bu durum da Schrödinger denklemlerini çözülemez hale getirir. Bu sebeple çok parçacık probleminin çözülebilmesi için zaman içinde birtakım yaklaşımlar yapılmıştır. Born-Oppeinheimer, Hartree, Hartree-Fock yaklaşımları ile denklem bir parça kolaylaşmışsa da çözüm sağlanamamıştır. Bu yaklaşımlar, elektronların kendileri ve dalga fonksiyonlarına bağlı çözüm önermekte olduklarından ancak bir noktaya kadar kolaylık sağlayabilmişlerdir. Thomas-Fermi ile birlikte temel değişken electron yoğunluğu olarak ele alınmıştır. Ardından Hohenmerg-Kohn buna dayalı iki temel teorem ve çözümünü ortaya atmış ve Yoğunluk Fonksiyoneli Teorisinin temellerini oluşturmuşlardır. Ardından Kohn-Sham denklemleri ile iterasyon yöntemle çözülebilen Yoğunluk Fonksiyoneli Teoremi oluşturulmuş, böylece zamandan bağımsız Schrödinger denklemi yerine Kohn-Sham denklemleri kullanılarak çok parçacık problemi çözülebilir hale getirilmiştir.

Bu çalışmada Yoğunluk Fonksiyoneline Dayalı olarak hesap yapan ABINIT bilgisayar programı kullanılarak, Genelleştirilmiş Gradyent Yaklaşımı ve Yerel Yoğunluk Yaklaşımları altında $BaIrO_3$ kristalinin yapısal, elektronik ve elastik özellikleri incelenmiştir.

ABINIT yazılım projesi, birçok farklı grupların uluslararası işbirliğini sağlamak için çeşitli yazılım mühendisliği teknikleri kullanılarak geliştirilen, herkese açık yazılım projesi olarak 1997 yılında Xavier GONZE ve arkadaşları tarafından başlatıldı. ABINIT paketinin ana programı, düzlemsel dalga temeli ve pseudo potansiyeller kullanarak malzeme özelliklerinin yoğunluk fonksiyonel hesaplamalarını gerçekleştirir (Gonze ve ark., 2002).

ABINIT, malzemelerin fiziksel özelliklerini hesaplamak için kullanılan bir programdır. ABINIT in öğretilmesi için çevrimiçi eğitimler verilmektedir (www.abinit.org/.)

ABINIT 2000 yılında araştırmacıların kullanımına açıldı. Böylece açık kaynak haline getirilerek, kullanıcılar tarafından da yenilenmesi ve geliştirilmesi sağlanmıştır. Yine web sitesindeki psodö-potansiyeller kullanılarak iterasyonla hesaplamalar yapmakta ve malzemelerin fiziksel özelliklerini oldukça yüksek bir doğrulukla elde edilmesini sağlamaktadır.

2. BULGULAR VE TARTIŞMA

2.1. $BaIrO_3$ Kristalinin Özellikleri

$BaIrO_3$ kristalinin kübik ve monoklinik olmak üzere iki yapısı vardır. Bu çalışmada kübik yapı incelenmiştir. Adı Baryum Iridyum Oksittir. Uzay grubu $Pm\bar{3}m$ (No:221), nokta grubu ise $m\bar{3}m$ dir. Kübik yapıdaki $BaIrO_3$ perovskit kristaldir.

2.2. $BaIrO_3$ Kristalinin Yapısal Özellikleri

Yapısal özelliklerin hesaplanması ABINIT, bağ yapısı ve birim hücre hesaplamaları VESTA programları ile yapılmıştır. Kesme enerjisi 1088.46 eV, k noktaları için Monkhorst-Pack bölümlemesi 14x14x14 olarak saptanmıştır. Hacim optimizasyonu yapılarak $BaIrO_3$ kübik kristalinin örgü parametresi teorik olarak her iki yaklaşım altında hesaplanmıştır. Hesaplanan örgü parametresi değerlerinden yerel yoğunluk yaklaşımı altında elde edilen sonuç literatürdeki değere daha yakın bulunmuştur. Yine bu aşamada kristalin kararlı olduğu toplam enerjisi GGA yaklaşımı altında -69.59 Ha ve LDA yaklaşımı altında -69.71 Ha bulunmuştur (Çizelge 2.1). Hacim optimizasyonuyla son olarak kristalin basınç - hacim, toplam enerji-basınç ve toplam enerji hacim davranışları hesaplanmış ve grafiklerle ifade edilmiştir.

Çizelge 2.1. $BaIrO_3$ kristaline ait hesaplanmış örgü parametresi, hacim ve toplam enerji değerleri

	GGA	LDA	Literatür (Jain ve ark., 2013)
Örgü Parametresi (Bohr)	7.8389	7.6709	7.7049
Hacim ($Bohr^3$)	481.69	451.38	457.40
Toplam Enerji (eV)	-1893.6402	-1896.9056	---

2.3. $BaIrO_3$ Kristalinin Elektronik Özellikleri

$BaIrO_3$ kristalinin elektronik özelliklerinin ortaya konabilmesi için bu aşamada, kristale ait elektronik bant yapısı, durum yoğunluğu ve kismi durum yoğunlukları GGA ve LDA yaklaşımları altında hesaplanmış ve grafikleri çizdirilmiştir.

2.3.1. Elektronik bant yapısı

Elektronik bant grafiği $\Gamma - X - M - \Gamma - R - X$ yüksek simetri noktaları boyunca hesaplanmıştır. Fermi enerjisi 0 eV değerine çakıştırılmış ve grafiklerde kırmızı çizgilerle gösterilmiştir. Fermi seviyesinin altında valans bantları üstünde ise iletim bantları gözükmektedir. Valans bantlarından -20 eV enerji değerindekilerinin kor elektronlardan geldiği anlaşılmaktadır.

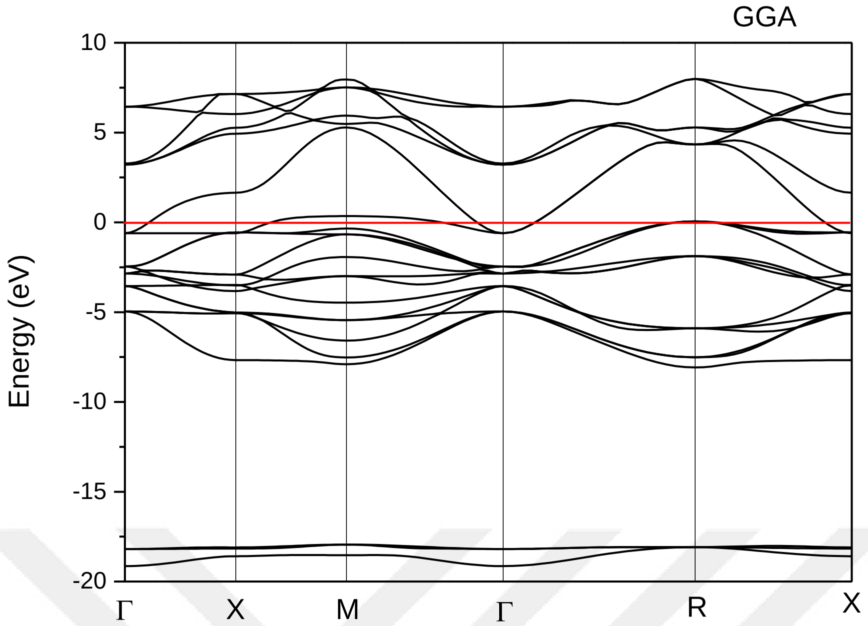

Şekil 2.1. $BaIrO_3$ kristalinin GGA yaklaşımı altındaki elektronik bant yapısı grafiği.

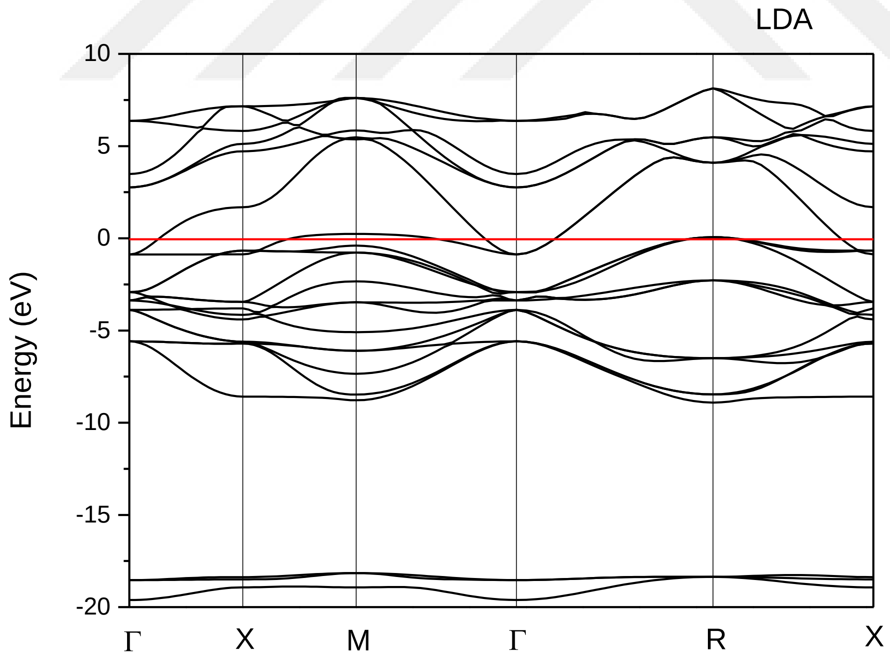

Şekil 2.2. $BaIrO_3$ kristalinin LDA yaklaşımı altındaki elektronik bant yapısı grafiği.

Her iki elektronik bant grafiğinden bu kristalin metal olduğu ve yüksel elektronik iletkenliğe sahip olduğu görülmüştür.

2.3.2. Durum yoğunluğu (DOS)

Durum yoğunluğu grafikleri her iki yaklaşım altında elde edilmiştir. Sonuçta iki yaklaşımla elde edilen sonuçların birbirleriyle ve elektronik bant yapısı grafikleriyle uyum içinde oldukları görülmüştür.

Durum yoğunluğu grafiklerinde yine Fermi seviyesi belirtilmiştir. Bu seviyenin altındaki enerji değerlerinde valans bantlarından gelen toplam katkı, üstündeki enerjilerde ise iletim bantlarından gelen katkılar görülür. Durum yoğunlukları keyfi birimlerde verilmiştir.

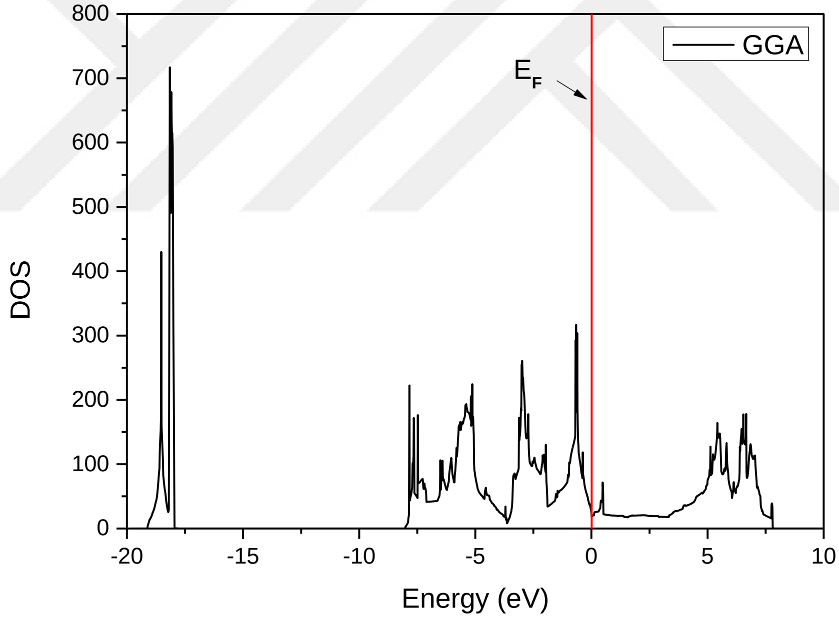

Şekil 2.3. $BaIrO_3$ kristalinin GGA yaklaşımı altındaki toplam durum yoğunluğu.

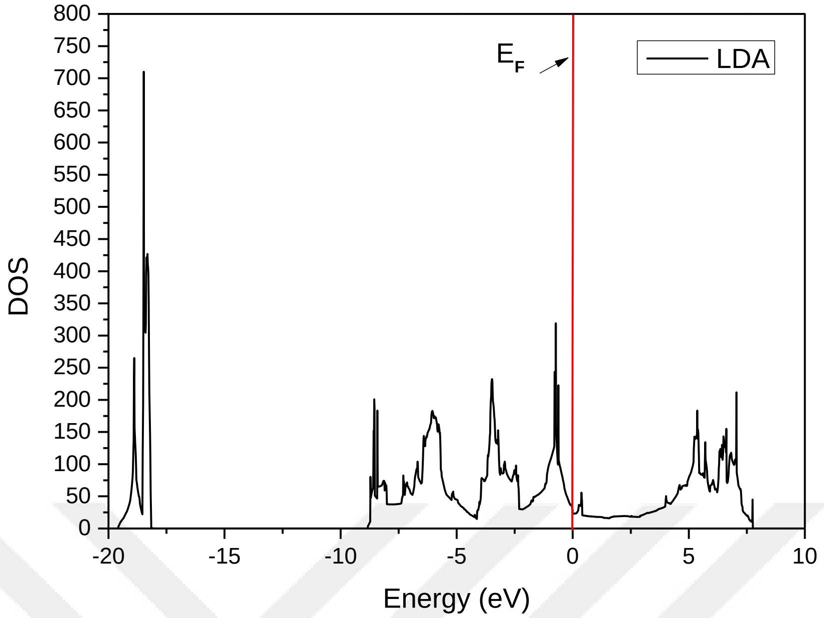

Şekil 2.4. $BaIrO_3$ kristalinin LDA yaklaşımı altındaki toplam durum yoğunluğu.

2.3.3. Kısmı durum yoğunlukları (PDOS)

Kristali oluşturan her farklı elemente ait atomun durum yoğunluğuna kısmi durum yoğunluğu denir. Burada Ba, Ir, O(1), O(2) ve O(3) atomlarına ait kısmi durum yoğunlukları GGA ve LDA yaklaşımları altında hesaplanmıştır. Kısmı durum yoğunluğu grafiklerinde gelen katkıların hangi seviyelerden (s, p, d ve/veya f) geldikleri de belirtilmiştir.

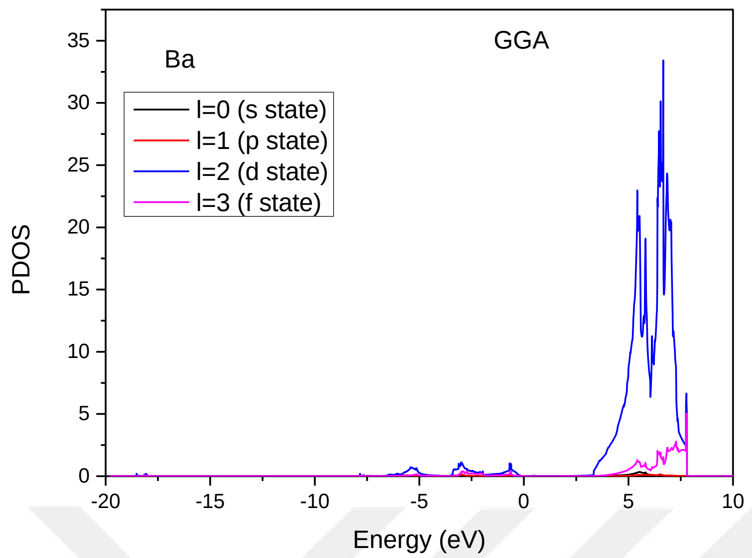

Şekil 2.5. Ba atomuna ait GGA yaklaşımı altındaki kısmı durum yoğunluğu.

Burada sadece Ba atomuna ait GGA yaklaşımı altındaki kısmi durum yoğunluğu grafiği verilmiştir. Diğer tüm atomların GGA ve LDA yaklaşımı altındaki kısmi durum yoğunluğu grafikleri tezin ilgili bölümünde yer almaktadır.

2.4. $BaIrO_3$ Kristalinin Elastik Özellikleri

$BaIrO_3$ kristalinin elastik yapısının anlaşılabilmesi için öncelikle elastik sertlik (C_{ij}) ve elastik uyum (S_{ij}) katsayıları hesaplanmıştır. $BaIrO_3$ kübik bir kristal olduğundan ve kübik kristallerin simetri özelliğinden dolayı elastik sertlik ve uyum katsayılarının sadece üç bileşenleri bulunmaktadır. Söz edilen değerler Çizelge 2.2 ve 2.3 de verilmiştir.

Çizelge 2.2. Elastik sertlik katsayıları

Elastik sertlik katsayıları	GGA (GPa)	LDA (GPa)
C_{11}	247.65	298.82
C_{12}	115.59	130.90
C_{44}	71.02	79.91

Çizelge 2.3. Elastik uyum katsayıları

Elastik uyum katsayıları	GGA $(GPa)^{-1}$	LDA $(GPa)^{-1}$
S_{11}	0.0040	0.0033
S_{12}	0.0086	0.0076
S_{44}	0.0140	0.0125

$BaIrO_3$ kristalinin mekanik olarak kararlı olup olmadığını anlayabilmek için Born kararlılık kriterlerine uyup uymadığına bakılmıştır (Mouhat ve ark. 2014). Kararlılık koşulları aşağıda verilmektedir.

$$C_{11} + 2C_{12} > 0,\ C_{44} > 0,\ \ C_{11} - C_{12} > 0\ ,\ \ \ C_{11} > 0 \text{ and } C_{12} < B < C_{11}$$

Burada B bulk modülüdür. $BaIrO_3$ tüm bu koşulları sağladığından mekanik olarak kararlı olduğu anlaşılmaktadır.

Ardından elde edilen değerler kullanılarak Bulk, kesme ve young modülleri ile, Poisson oranı, esneklik katsayısı, Zener anizotropi faktörleri hesaplanmıştır (Çizelge 2.4).

Çizelge 2.4. $BaIrO_3$ kristaline ait GGA ve LDA yaklaşımları altında hesaplanmış olan temel elastik özellikleri

Elastik Özellikler	Sembol (Birim)	GGA	LDA
Voight Bulk Modülü	B_V (GPa)	159.61	186.88
Reuss Bulk Modülü	B_R (GPa)	159.61	186.88

Hill Bulk Modülü	B_H (GPa)	159.61	186.88
Voight Shear Modülü	G_V (GPa)	69.03	81.54
Reuss Shear Modülü	G_R (GPa)	68.94	81.49
Hill Shear Modülü	G_H (GPa)	68.98	81.51
Young Modülü	E (GPa)	180.89	213.49
Poisson Oranı	v (-)	0.311	0.310
Esneklik Katsayısı	$K=B_{VRH}/G_{VRH}$ (-)	2.314	2.293
Zener Anizotropi Faktörü	A (-)	1.00	0.95

Hesaplanan Poisson oranının 0.26 dan yüksek çıkması ve yine hesaplanan esneklik katsayısının 1.75 den büyük çıkması $BaIrO_3$ kristalinin elastik yani esnek bir malzeme olduğunu göstermektedir. Zener anizotropi katsayısının 1 e çok yakıl olmasıyla bu kristalin izotropik kristal olduğu anlaşılmaktadır.

3. SONUÇ

Bu tez çalışmasında $BaIrO_3$ kristalinin yapısal, elektronik ve elastik özellikleri Yoğunluk Fonksiyoneli Teorisine bağlı olarak çalışan ABINIT bilgisayar programıyla genelleştirilmiş gradyent ve yerel yoğunluk yaklaşımları altında hesaplanmıştır.

İlk olarak kesme enerjisi ve k noktalarının sayısı belirlenmiştir. Bu değerler bu aşamadan sonraki tüm hesaplamalarda kullanılmıştır. $BaIrO_3$ kristalinin yapısal özellikleri örgü parametresinin teorik değerinin hesaplanmasıyla ortaya konulmaya başlanmıştır. Bu aşamada kristalin taban durumda kararlı olduğu toplam enerji değeri, toplam enerji-basınç, toplam enerji-hacim ve basınç-hacim davranışları incelenmiş ve grafiklerle ortaya konulmuştur. $BaIrO_3$ kristalinin bağ yapıları, bağ uzunlukları ve birim hücre görüntüsü VESTA bilgisayar programıyla elde edilmiştir. Ardından elektronik bant yapısı, toplam ve kısmi durum yoğunlukları hesaplanarak ve grafikleri çizdirilerek, $BaIrO_3$ kristalinin elektronik iletkenliği yüksek bir metal olduğu anlaşılmıştır.

Çalışmanın son aşamasında ise kristalin elastic sertlik, elsatik uyum katsayıları ve Bulk, Shear, Young Modülleri, Poisson oranı, Esneklik katsayısı ve Zener anizotropi katsayıları hesaplanmıştır. Elde edilen değerler $BaIrO_3$ kristalinin mekanik olarak kararlı ve esnek bir yapıda olduğunu ortaya koymuştur.

Elde edilen sonuçlardan sadece örgü parametresi değeri literatürle karşılaştırılmış ve oldukça yakın sonuç bulunduğu görülmüştür. Bundan başka $BaIrO_3$ kristali hakkında bu alanda çalışma bulunmamaktadır. Bu nedenle, bu tez çalışmasının $BaIrO_3$ üzerine gerçekleştirilecek çalışmalara ışık tutacağı düşünülmektedir.

UNIVERSITY OF VAN YUZUNCU YIL
THE ISTITUTE OF NATURAL AND APPLIED SCIENCES
THESIS ORIGINALITY REPORT

Date: 14/09/2021

Thesis Title: **THE INVESTIGATION OF SOME PHYSICAL PROPERTIES OF $BaIrO_3$ PEROVSKITE CRYSTAL WITH DENSITY FUNCTIONAL THEORY.** The title of the mentioned thesis, above having total 91 pages with cover page, introduction, main parts and conclusion, has been checked for originality by Turnitin computer program on the date of 14/09/2021 and its detected similar rate was 12% according to the following specified filtering

Originality report rules:

- Excluding the Cover page,
- Excluding the Thanks,
-Excluding the Contents,
- Excluding the Symbols and Abbreviations,
- Excluding the Materials and Methods
- Excluding the Bibliography,
- Excluding the Citations,
- Excluding the publications obtained from the thesis,
- Excluding the text parts less than 7 words (Limit match size to 7 words)

I read the Thesis Originality Report Guidelines of Yuzuncu Yil University for Obtaining and Using Similarity Rate for the thesis, and I declare the accuracy of the information I have given above and my thesis does not contain any plagiarism; otherwise I accept legal responsibility for any dispute arising in situations which are likely to be detected.

Sincerely yours,

14/09/2021

Name and Surname: Hawzhi Rzgar SOR

Student ID#: 18910001390

Science: Physics

Program: Master

Statute: M. Sc. X Ph.D. ☐

APPROVAL OF SUPERVISOR
SUITABLE

APPROVAL OF THE INSTITUTE
SUITABLE

Assoc. Prof. Dr. Emel KILIT DOĞAN